Research Article
NAFLD and Alcohol-Related Liver Diseases

JOURNAL
OF HEPATOLOGY

Intestinal B cells license metabolic T-cell activation in NASH microbiota/antigen-independently and contribute to fibrosis by IgA-FcR signalling

Authors

Elena Kotsiliti, **Valentina Leone**, Svenja Schuehle, …, Frank Tacke, Quentin M. Anstee, Mathias Heikenwalder

Correspondence

m.heikenwaelder@dkfz.de, Mathias.Heikenwaelder@med.uni-tuebingen.de (M. Heikenwalder).

Graphical abstract

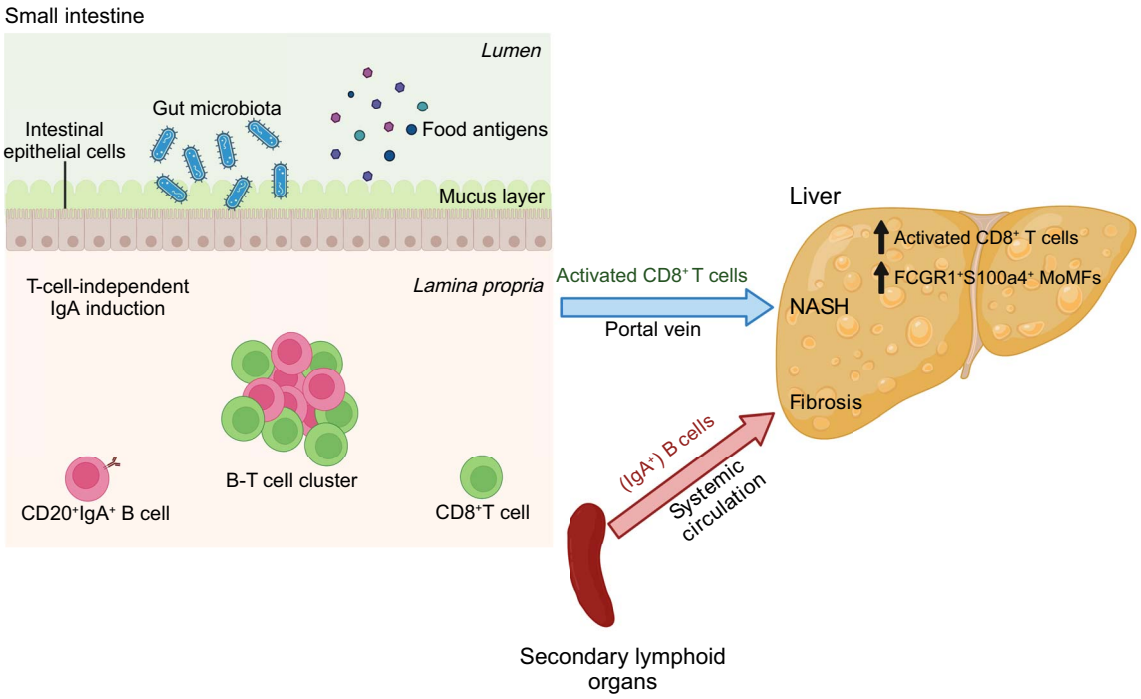

Highlights

- Intestinal B cells are metabolically activated in NASH mouse models, and increased in murine and human NASH.
- NASH intestinal B cells are activated independently of the gut microbiota.
- B cells promote metabolic T-cell activation in the gastrointestinal tract independently of TCR signalling.
- IgA secretion and FcRγ signalling on MoMFs/SAMacs aggravate hepatic fibrosis in mice and patients with NASH.
- Genetic and therapeutic B-cell abrogation reduced T-cell-driven inflammation and fibrosis in NASH.

Impact and Implications

There is currently no effective treatment for non-alcoholic steatohepatitis (NASH), which is associated with a substantial healthcare burden and is a growing risk factor for hepatocellular carcinoma (HCC). We have previously shown that NASH is an auto-aggressive condition aggravated, amongst others, by T cells. Therefore, we hypothesized that B cells might have a role in disease induction and progression. Our present work highlights that B cells have a dual role in NASH pathogenesis, being implicated in the activation of auto-aggressive T cells and the development of fibrosis via activation of monocyte-derived macrophages by secreted immunoglobulins (*e.g.*, IgA). Furthermore, we show that the absence of B cells prevented HCC development. B cell-intrinsic signalling pathways, secreted immunoglobulins, and interactions of B cells with other immune cells are potential targets for combinatorial NASH therapies against inflammation and fibrosis.

https://doi.org/10.1016/j.jhep.2023.04.037
 J. Hepatol. 2023, 79, 296–313

Research Article
NAFLD and Alcohol-Related Liver Diseases

JOURNAL
OF HEPATOLOGY

Intestinal B cells license metabolic T-cell activation in NASH microbiota/antigen-independently and contribute to fibrosis by IgA-FcR signalling

Elena Kotsiliti[1,†], **Valentina Leone**[1,2,3,43,†], Svenja Schuehle[1,41,#], Olivier Govaere[4,#], Hai Li[5], Monika J. Wolf[31,§], Helena Horvatic[6], Sandra Bierwirth[7,8], Jana Hundertmark[9], Donato Inverso[10,11], Laimdota Zizmare[12], Avital Sarusi-Portuguez[13], Revant Gupta[14,15], Tracy O'Connor[1,42], Anastasios D. Giannou[16,17], Ahmad Mustafa Shiri[16], Yehuda Schlesinger[13], Maria Garcia Beccaria[1], Charlotte Rennert[17], Dominik Pfister[1], Rupert Öllinger[3], Iana Gadjalova[18], Pierluigi Ramadori[1], Mohammad Rahbari[1], Nuh Rahbari[19], Marc E. Healy[21], Mirian Fernández-Vaquero[1], Neda Yahoo[1], Jakob Janzen[1], Indrabahadur Singh[1,39], Chaofan Fan[1], Xinyuan Liu[20,21], Monika Rau[22], Martin Feuchtenberger[23], Eva Schwaneck[24], Sebastian J. Wallace[25], Simon Cockell[40], John Wilson-Kanamori[25], Prakash Ramachandran[25], Celia Kho[6], Timothy J. Kendall[25,26], Anne-Laure Leblond[31], Selina J. Keppler[18], Piotr Bielecki[27], Katja Steiger[28,29], Maike Hofmann[14], Karsten Rippe[30], Horst Zitzelsberger[2], Achim Weber[31], Nisar Malek[32], Tom Luedde[33], Mihael Vucur[33], Hellmut G. Augustin[10,11], Richard Flavell[27], Oren Parnas[11], Roland Rad[3,18], Olivier Pabst[34], Neil C. Henderson[25,26], Samuel Huber[16], Andrew Macpherson[5], Percy Knolle[35], Manfred Claassen[14,15,32], Andreas Geier[22], Christoph Trautwein[12], Kristian Unger[2], Eran Elinav[36,37], Ari Waisman[20,21], Zeinab Abdullah[6], Dirk Haller[7,8], Frank Tacke[9], Quentin M. Anstee[4,38], Mathias Heikenwalder[1,44,*]

Journal of Hepatology **2023**. vol. 79 | 296–313

Background & Aims: The progression of non-alcoholic steatohepatitis (NASH) to fibrosis and hepatocellular carcinoma (HCC) is aggravated by auto-aggressive T cells. The gut-liver axis contributes to NASH, but the mechanisms involved and the consequences for NASH-induced fibrosis and liver cancer remain unknown. We investigated the role of gastrointestinal B cells in the development of NASH, fibrosis and NASH-induced HCC.

Methods: C57BL/6J wild-type (WT), B cell-deficient and different immunoglobulin-deficient or transgenic mice were fed distinct NASH-inducing diets or standard chow for 6 or 12 months, whereafter NASH, fibrosis, and NASH-induced HCC were assessed and analysed. Specific pathogen-free/germ-free WT and μMT mice (containing B cells only in the gastrointestinal tract) were fed a choline-deficient high-fat diet, and treated with an anti-CD20 antibody, whereafter NASH and fibrosis were assessed. Tissue biopsy samples from patients with simple steatosis, NASH and cirrhosis were analysed to correlate the secretion of immunoglobulins to clinicopathological features. Flow cytometry, immunohistochemistry and single-cell RNA-sequencing analysis were performed in liver and gastrointestinal tissue to characterise immune cells in mice and humans.

Results: Activated intestinal B cells were increased in mouse and human NASH samples and licensed metabolic T-cell activation to induce NASH independently of antigen specificity and gut microbiota. Genetic or therapeutic depletion of systemic or gastrointestinal B cells prevented or reverted NASH and liver fibrosis. IgA secretion was necessary for fibrosis induction by activating CD11b+CCR2+F4/80+CD11c-FCGR1+ hepatic myeloid cells through an IgA-FcR signalling axis. Similarly, patients with NASH had increased numbers of activated intestinal B cells; additionally, we observed a positive correlation between IgA levels and activated FcRg+ hepatic myeloid cells, as well the extent of liver fibrosis.

Conclusions: Intestinal B cells and the IgA-FcR signalling axis represent potential therapeutic targets for the treatment of NASH.

Keywords: NAFLD; NAFL; NASH; HCC; fibrosis; B cells; gut-liver axis.
Received 2 February 2023; received in revised form 5 April 2023; accepted 11 April 2023; available online 22 May 2023
* Corresponding author. Address: Department Chronic Inflammation and Cancer, German Cancer Research Center (DKFZ), Im Neuenheimer Feld 242, Heidelberg, 69120, Germany; Tel.: +49 6221 42-3890.
E-mail addresses: m.heikenwaelder@dkfz.de, Mathias.Heikenwaelder@med.uni-tuebingen.de (M. Heikenwalder).
§ Current address: Roche Pharmaceutical Research and Early Development Oncology, Roche Innovation Center Munich, Penzberg, Germany
† These authors contributed equally: Elena Kotsiliti & Valentina Leone
# These authors contributed equally: Svenja Schuehle & Olivier Govaere
https://doi.org/10.1016/j.jhep.2023.04.037

Introduction

The worldwide increase in obesity is driving an epidemic of non-alcoholic fatty liver disease (NAFLD), a progressive disease strongly associated with metabolic syndrome and characterised by excessive hepatic lipid accumulation, hepatocyte damage, and aberrant metabolism.[1,2] NAFLD is subdivided into simple steatosis and non-alcoholic steatohepatitis (NASH), an inflammatory, auto-aggressive[3,4] disease aggravated by T cells causing necro-inflammation.[5] Fibrosis, which can develop concomitantly with NASH, may progress to cirrhosis, increasing the risk of liver failure or liver cancer, the latter being the third most common cause of cancer-related death worldwide.[6] Hepatocellular carcinoma (HCC), the most frequent form of primary liver cancer,[7] is highly linked to the pathological background of NAFLD.[2] Fibrosis is a critical factor for predicting disease outcome as it correlates with the increased risk of HCC mortality in patients with NASH[8,9]. It has also been reported that in a subset of patients, NASH-driven HCC occurs in the absence of severe fibrosis/cirrhosis.[2,10] Consequently, there is a considerable healthcare cost burden owing to NASH, including HCC surveillance.[11–13]

The gut-liver axis is a critical component in NAFLD pathogenesis.[14] Animal studies have demonstrated a direct role of altered intestinal microbiota in steatosis,[15] NASH(16), fibrosis[17] and liver cancer.[18] In addition, sterile inflammation, mediated by damage-associated molecular patterns and metabolite-associated molecular patterns,[19,20] is considered an important driver of liver injury in NASH. Moreover, macrophages play a crucial role in liver injury and fibrosis in NASH, with monocyte-derived macrophages (MoMFs) exhibiting a proinflammatory phenotype that can directly activate hepatic stellate cells.[21]

Serum IgA, secreted by plasma cells in secondary lymphoid organs, has been shown to be elevated in patients with NAFLD,[22,23] and was an independent predictor of advanced fibrosis.[22] Chronic inflammation and fibrosis in humans and mice with NAFLD were accompanied by liver-resident immunoglobulin A (IgA)-producing programmed death-ligand 1-positive cells suppressing efficient anti-liver cancer immune responses.[24] In a mouse model of NASH, it was shown that intrahepatic B cells, activated by gut-derived microbial factors, contributed to hepatic inflammation and fibrosis,[25] while another mouse study demonstrated that intrahepatic regulatory B cells were involved in disease pathogenesis.[26] Moreover, further studies have shown a role of IgA in liver diseases, such as alcohol-related liver disease and NAFLD/NASH[27]. However, the exact role and origin of B cells in NASH, and the involvement of B cells in T-cell activation and fibrosis initiation and/or development, remain unclear. Herein, we report that intestinal $CD20^+$ B cells and immunoglobulin secretion are involved in the pathogenesis of NASH in mice and humans and that peripheric IgA^+ and MoMFs-FcRγ signalling contribute to NASH-induced liver fibrosis.

Material and methods

Details on the materials and methods are provided in the supplementary information and the supplementary CTAT table.

Results

B cells are required for NASH and NASH-driven HCC in mice

To investigate the role of systemic B cells in NASH, C57BL/6J wild-type (WT) littermates and B cell-deficient ($JH^{-/-}$) mice[28] were fed a NASH-inducing choline-deficient high-fat diet (CD-HFD) for 6 or 12 months. As previously described, WT CD-HFD mice developed NASH (after approx. 6 months – 100% penetrance) and HCC (approx. 30% incidence at 12 months post-diet-start), recapitulating several clinical features of human disease.[29] $JH^{-/-}$ CD-HFD mice gained significantly more weight than normal chow-fed (ND) controls at around 9 months of age, reaching the same body weight as WT CD-HFD mice at 12 months post-diet-start (Fig. S1B). $JH^{-/-}$ CD-HFD mice lacked liver steatosis and had a low NAFLD activity score (NAS) after 6 months (Fig. 1A,B and Fig. S1A) and 12 months on diet (Fig. S1G,H). High serum alanine aminotransferase (ALT) values, typically seen in WT CD-HFD mice, were low in $JH^{-/-}$ CD-HFD serum at 6 (Fig. 1C and Fig. S1A) and 12 months (Fig. S1G). Serum cholesterol and hepatic triglyceride levels were lower in $JH^{-/-}$ than in WT CD-HFD mice at both time points (Fig. S1A,G), with a substantial decrease in hepatic large lipid droplets (Fig. 1D). Intraperitoneal glucose tolerance test revealed normal insulin response in $JH^{-/-}$ CD-HFD mice, contrary to WT CD-HFD mice (Fig. S1C). Flow cytometry analyses showed significantly fewer $CD3^+$ and $CD8^+$ T cells in $JH^{-/-}$ CD-HFD livers than in WT (Fig. S1E) and confirmed the absence of $CD19^+$ B cells (Fig. S1F). A similar reduction in $CD3^+$ cells was observed by immunohistochemistry (IHC) analysis of $JH^{-/-}$ CD-HFD liver sections (Fig. S1D). Hepatic $CD8^+$ $CD62L^-$ activated T cells TNF and IFNγ-producing $CD8^+$ cells were decreased (Figs. 1E-G) similarly to myeloid cells, as seen by staining for $F4/80^+$ cells and MHC-II^+ aggregates (Fig. S1D). $P62^+$, cleaved Caspase 3^+ cells, and $PD1^+$ cells were increased in WT CD-HFD livers compared to WT ND but remained significantly lower in $JH^{-/-}$ CD-HFD livers (Fig. S1D).[3,30]

To evaluate the importance of B cells in NASH, we therapeutically depleted B cells using anti-CD20 monoclonal antibodies (αCD20 mAb) in WT mice with NASH fed a CD-HFD for 4 months (Fig. 1H). Before treatment, we confirmed NASH 4 months post diet-start in mice from the identical mouse cohort (Fig. S1J,K). B-cell depletion was performed for 6 weeks on CD-HFD mice, and depletion efficacy was evaluated in the liver, small intestine (Peyer's patches removed) (Fig. 1I,J), the spleen, and blood (Fig. S1N,O). In agreement with the genetic model, WT CD-HFD αCD20 mAb-treated mice lacked NASH (Figs. 1K,L and Fig. S1I), and ALT serum levels were significantly reduced compared to controls (isotype control-treated or untreated WT CD-HFD mice) (Fig. 1M and Fig. S1I). WT CD-HFD αCD20 mAb-treated mice showed lower body weight at the endpoint (Fig. S1L) and a strong reduction of hepatic large lipid droplets (Fig. 1N). Accordingly, hepatic triglycerides and serum cholesterol were decreased (Fig. 1O and Fig. S1I). Intraperitoneal glucose tolerance test revealed impaired insulin responses in the αCD20 mAb-treated mice, similar to WT CD-HFD (Fig. S1M). B-cell depletion reduced the accumulation of hepatic $CD3^+$, $CD8^+$ (Fig. S1P,Q), $CD8^+$ $CD62L^-$, $CD8^+$ TNF^+

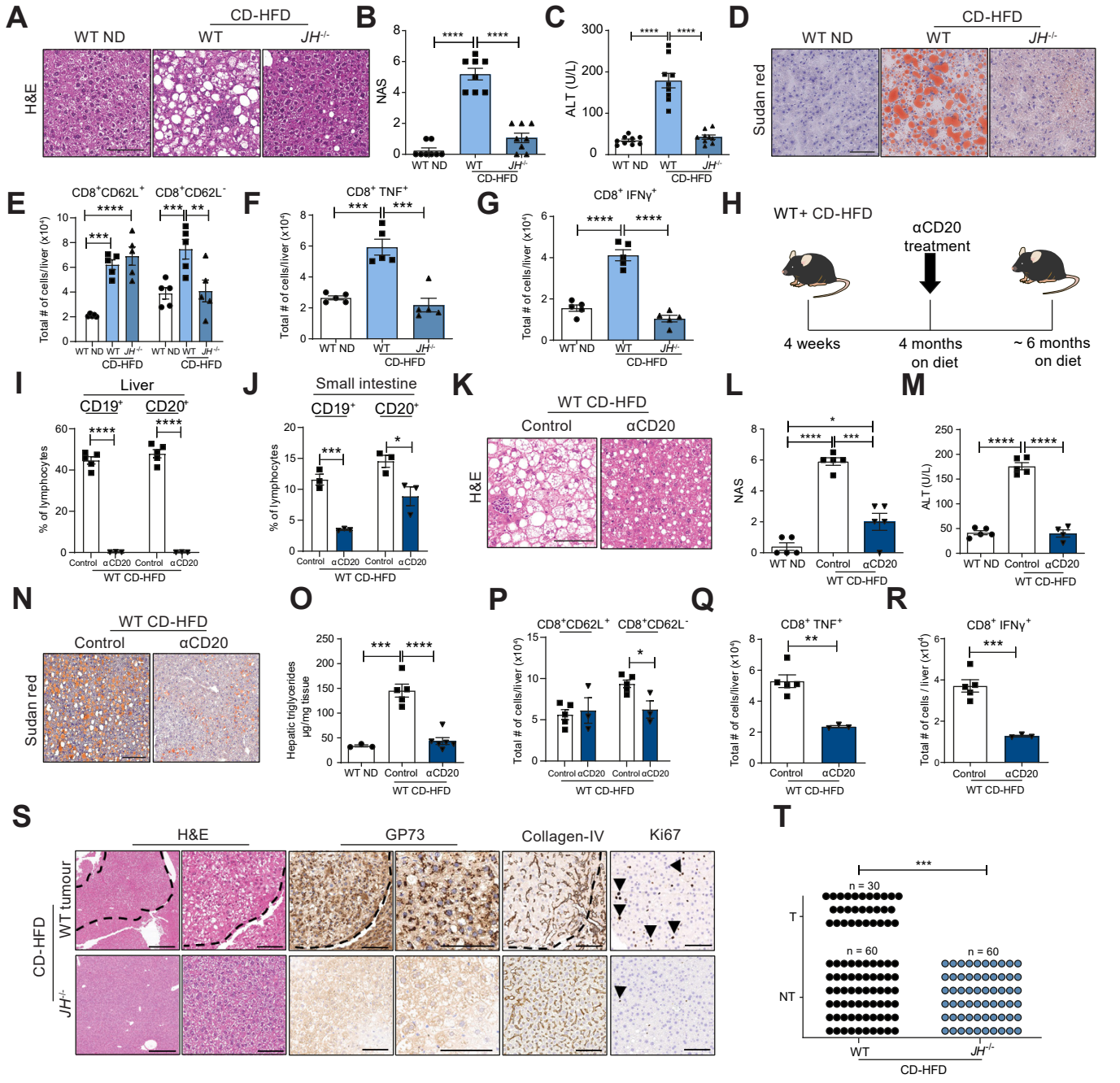

Fig. 1. B cells support NASH and subsequent HCC development. (A) Representative H&E staining of liver sections derived from WT ND, CD-HFD and *JH*$^{-/-}$ CD-HFD male mice fed for 6 months. (B) NAFLD score evaluation (n = 8). (C) Serum ALT levels (n = 9). (D) Representative Sudan red analysis of liver sections of male mice fed for 6 months. (E-G) Quantifications of the total number of cells (absolute number) of liver flow cytometry analyses of male mice (n = 5) fed for 6 months (numbers indicate %) of (E) hepatic CD8$^+$CD62L$^+$ and CD8$^+$CD62L$^-$ T cells, (F) CD8$^+$TNF$^+$ cells, (G) CD8$^+$IFNγ$^+$ cells, derived from livers of the respective genotypes/groups fed for 6 months. (H) Treatment scheme for the WT CD-HFD male mice treated with B-cell depletion antibody anti-CD20 (αCD20). (I) Quantifications of flow cytometry analyses of liver CD19$^+$ and CD20$^+$ cells and (J) lamina propria small intestine CD19$^+$ and CD20$^+$ cells, comparing control and WT CD-HFD αCD20-treated male mice (n ≥3). All mice were fed for 6 months. (K) Representative H&E staining of liver sections. (L) NAS evaluation of mice (n = 5). (M) Serum ALT levels in male mice (n = 5). (N) Representative Sudan red staining of liver sections of control and WT CD-HFD αCD20-treated male mice. (O) Analysis of hepatic triglycerides in male mice (n ≥3). (P–S) Quantification of flow cytometry analyses comparing control-treated and WT CD-HFD αCD20-treated male mice (n ≥3) of (P) hepatic CD8$^+$CD62L$^+$ and CD8$^+$CD62L$^-$ cells; quantification of (Q) hepatic CD8$^+$TNF$^+$ cells and (R) CD8$^+$IFNγ$^+$ cells. (S) Representative H&E staining and IHC staining of GP73, collagen IV and Ki67 for WT CD-HFD tumours and for not-affected livers of *JH*$^{-/-}$ CD-HFD; from 12 months fed CD-HFD mice. Scale bars represent H&E: 500 µm (left) and 100 µm (right); GP73: 100 µm; collagen IV: 100 µm; Ki67: 100 µm (positive hepatocytes depicted by arrowheads). (T) Graph summarizing non-tumour (NT) and tumour (T), of WT and *JH*$^{-/-}$ mice fed with CD-HFD for 12 months (numbers of mice are indicated, as symbols depict individual mice), data were analysed by Fisher's exact test. All data are presented as mean ± SEM. Statistical analyses were performed using unpaired *t* test. Displayed scale bars represent 100 µm.

and CD8$^+$ IFNγ^+ cells (Fig. 1P-R). IHC confirmed the efficient depletion of B220$^+$ cells and revealed decreased F4/80$^+$ cells and MHC-II$^+$ cell aggregates in WT CD-HFD αCD20 mAb livers (Fig. S1Q).

Metabolomic analysis revealed an altered metabolic hepatic profile of CD-HFD-treated mice in the absence of B cells (*e.g.*, triglycerides), both genetically and therapeutically. Hepatic deregulation of several lipid and cholesterol metabolism genes,

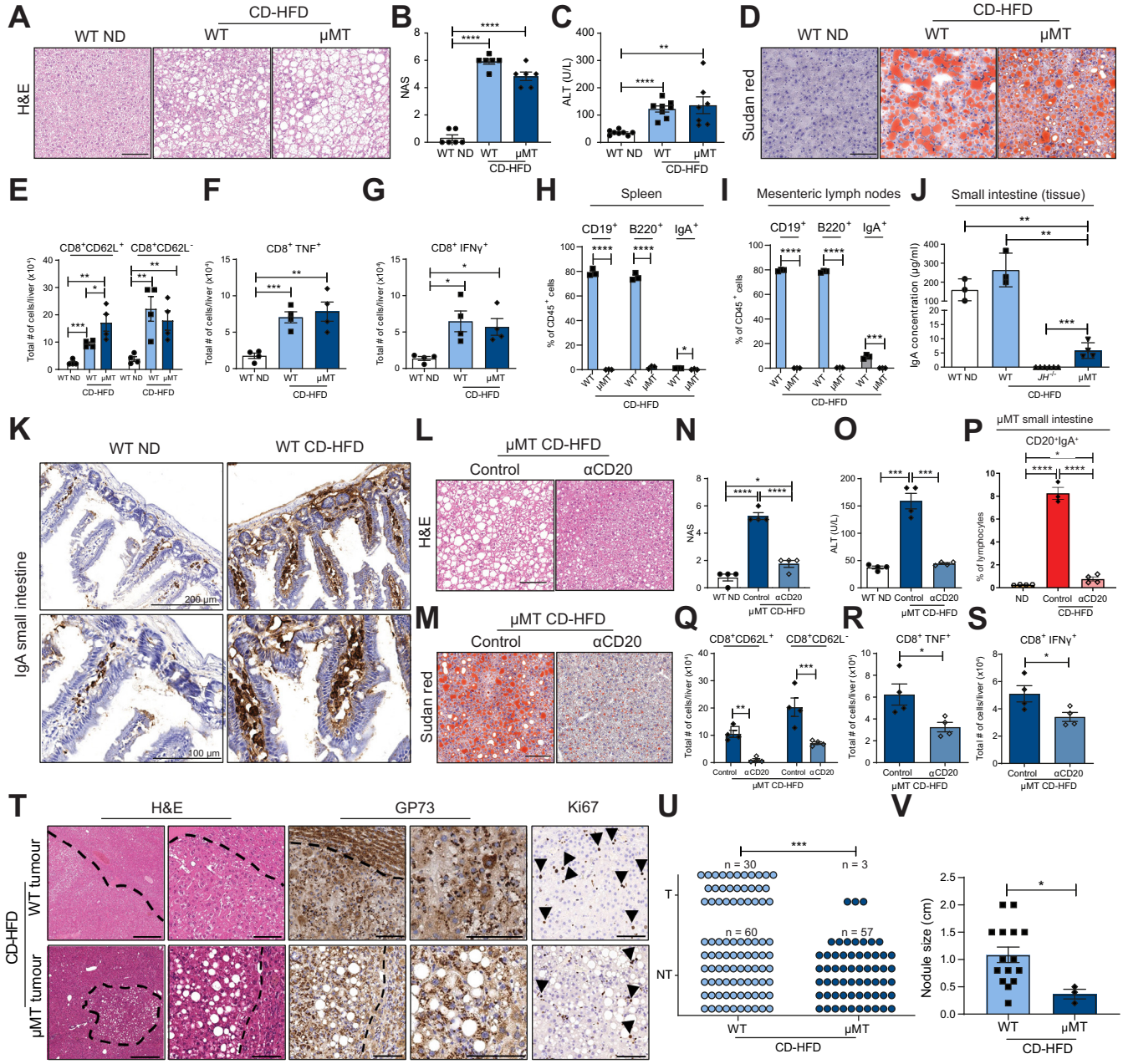

Fig. 2. Intestinal B cells suffice to cause NASH. (A) Representative H&E staining of liver sections of WT ND, WT and *μMT* CD-HFD male mice fed for 6 months. (B) NAS male mice (n = 6). (C) Serum ALT levels in male mice (n ≥6). (D) Representative Sudan red staining of liver sections. (E) Absolute quantifications of flow cytometry of hepatic CD8$^+$CD62L$^+$ and CD8$^+$CD62L$^-$ T cells, (F) for CD8$^+$TNF$^+$ cells and (G) CD8$^+$IFNγ^+ cells (n = 4). (H) Percentages of splenic CD19$^+$, B220$^+$ and IgA$^+$ cells in male mice (n = 3), evaluated by flow cytometry. (I) Percentages of CD19$^+$, B220$^+$ and IgA$^+$ cells from mesenteric lymph nodes of male mice (n = 3), evaluated by flow cytometry. (J) IgA levels of small intestinal tissues in male mice (n ≥3), measured by ELISA. (K) Representative IgA staining of small intestine sections of 6-month-old male mice (upper row: scale bar 200 μm, bottom row scale bar: 100 μm). (L) Representative H&E staining of liver sections of 6-month-old *μMT* CD-HFD and μMT CD-HFD αCD20-treated male mice. (M) Representative Sudan red staining of liver sections of male mice. (N) NAS evaluation of male mice (n = 4). (O) ALT levels in male mice (n = 4). (P) Flow cytometric analysis quantifications of lamina propria CD20$^+$IgA$^+$ cells. (Q) Absolute quantifications of hepatic CD8$^+$CD62L$^+$ and CD8$^+$CD62L$^-$ cells (n = 4). (R) Hepatic CD8$^+$TNF$^+$ and (S) CD8$^+$IFNγ^+ cells, comparing WT ND, *μMT* CD-HFD and *μMT* CD-HFD αCD20-treated male mice (n = 4). (T) Representative H&E and IHC staining of GP73 and Ki67 in WT and *μMT* CD-HFD tumours (12 months under diet). Scale bars H/E: 500 μm (left) and 100 μm (right); GP73: 100 μm; Ki67: 100 μm (positive hepatocytes depicted by arrowheads). (U) Graph summarizing non-tumour (NT) and tumour (T) of WT and *μMT* mice fed with CD-HFD for 12 months (n ≥60). Symbols depict individual mice. Data were analysed by Fisher's exact test. (V) Quantification of nodule size in 12-month WT and μMT CD-HFD mice (n ≥3). All data are presented as mean ± SEM. Statistical analyses were performed using unpaired *t* test. The scale bars represent 100 μm.

usually found in NASH livers,[3,20,29] was prevented in *JH*$^{-/-}$ CD-HFD mice (Fig. S1R). In addition, proton nuclear magnetic resonance (^{1}H-NMR) spectroscopy analyses identified altered liver lipids correlating with the absence of B cells (Fig. S1S).

Of 60 *JH*$^{-/-}$ CD-HFD mice at 12 months post-diet start, none displayed liver cancer, unlike WT CD-HFD mice, which developed HCC at an incidence of 30%[20,29] (Fig. 1S,T). Together, our data indicate a key role of systemic B-cell responses in the development and maintenance of NASH and NASH-driven HCC.

Small intestine B-cell responses are sufficient to induce NASH in mice

To investigate and further corroborate the role of intestinal B cells in NASH and liver fibrosis, we utilized a second B cell-deficient mouse model (*μMT* mice), lacking expression of membrane-bound immunoglobulin M (IgM) on B cells. μMT mice selectively develop IgA^{+} B cells without IgM or IgD heavy chain expression by using alpha rather than the mu constant region chain[31] and only develop in the gastrointestinal tract. CD-HFD *μMT* mice gained significantly more weight than controls (Fig. S2B) and developed comparable NASH levels as in WT CD-HFD at 6 (Fig. 2A, 2B and Fig. S2A) and 12 months post-diet start (Figs. S2O, S2P). Serum ALT and cholesterol levels of *μMT* CD-HFD mice were similar to WT CD-HFD at 6 and 12 months (Figs 2C and Fig. S2A,O). Accumulated hepatic lipid droplets and increased hepatic triglycerides were observed in *μMT* CD-HFD mice for both time points (Fig 2D and Fig. S2A,O). An increase in activated intrahepatic CD8^{+} T cells with elevated TNF^{+} and IFNγ^{+} expression, as well as an impaired insulin response, were observed in *μMT* CD-HFD mice (Fig. 2C,E-G). Due to their lack of follicular B cells (Fig. 2H,I and Fig. S2F), μMT CD-HFD spleens lacked structured architecture (*e.g.*, germinal centres) (Fig. S2D). Flow cytometry analysis of small intestines from *μMT* CD-HFD mice identified IgA^{+} B cells, contrary to *JH*$^{-/-}$ CD-HFD mice (Fig. S1G). WT CD-HFD mice exhibited increased IgA levels in the ileum of the small intestine compared with ND control mice; IgA was present at low levels in the small intestine of *μMT* CD-HFD mice but was absent in CD-HFD *JH*$^{-/-}$ mice (Fig. 2J,K). An abundance of IgA^{+}-coated bacteria in *μMT* faeces indicates a local secretion of IgA into the intestinal tract (Fig. S2K). Increased IgM and IgG2b found in the small intestine of WT-CD-HFD mice (Fig. S2H) were undetectable in both *JH*$^{-/-}$ and *μMT* mice. IHC analysis demonstrated a lack of intrahepatic B cells in *μMT* CD-HFD mice (Fig. S2L) and an increase in F4/80^{+} cells and MHC-II^{+} aggregates compared to ND mice (Fig. S2L), contrary to *JH*$^{-/-}$ CD-HFD mice. P62^{+} and cleaved caspase 3^{+} cells were increased in *μMT* CD-HFD mice, as in WT CD-HFD mice (Fig. S2L). Moreover, transcriptional analyses of *μMT* CD-HFD livers demonstrated altered expression of several genes involved in lipid and cholesterol metabolism (Fig. S2N).

To investigate whether the susceptibility of *μMT* mice to liver inflammation was due to B cells in the intestine, we depleted the latter following feeding with CD-HFD for 4 months in mice with established NASH (Fig. S2Q,R). αCD20-antibody treatment reversed NASH in *μMT* CD-HFD mice (Figs. 2L,N and Fig. S2S), which displayed slightly lower body weight at endpoint than the control-IgG-treated mice (Fig. S2T). Serum ALT and cholesterol levels were significantly reduced (Fig. 2O and Fig. S2S), large lipid droplets were strongly decreased (Fig. 2M), and hepatic triglycerides and serum cholesterol were significantly reduced in αCD20 antibody-treated mice (Fig. S2S). Flow cytometry analysis of small intestines from CD-HFD μMT mice revealed a significant increase in CD20^{+} IgA^{+} B cells compared with *μMT* ND-fed mice, highlighting the NASH-induced gastrointestinal B-cell accumulation, which was reduced by αCD20-antibody treatment (Fig. 2P and Fig. S2U). In addition, flow cytometry analysis revealed a strong decrease of hepatic CD3^{+}, CD8^{+} (Fig. S2W), CD8^{+} CD62L^{-}, and CD8^{+} TNF^{+} and CD8^{+} IFNγ^{+} cells in αCD20-treated *μMT* CD-HFD-fed mice (Fig. 2Q-2S). This observation was corroborated by IHC (Fig. S2V), which also revealed a reduction in F4/80^{+} cells and MHC-II^{+} aggregates in αCD20-treated *μMT* CD-HFD mice compared to controls.

Notably, of 60 μMT mice fed a CD-HFD for 12 months, only three mice displayed liver tumours (not HCC; incidence of ≤5%) contrary to WT CD-HFD mice, as also described in Fig. 1S (same control cohort) and with smaller nodule size than in WT (Fig. 2T-2V). Thus, we conclude that intestinal B cells suffice for the development of diet-induced NASH, yet tumour incidence is strongly reduced.

Intestinal B cells interact with CD8^{+} T cells

We performed a multi-parameter flow cytometry analysis of the small intestine with Peyer's patches removed to identify distinct gut B-cell populations correlated with NASH. In line with our previous data, increased B cells were found in WT CD-HFD compared with ND mice. Notably, B cells (approx. 10% of CD45^{+} cells) downregulated CD19^{+} but retained CD20^{+} expression in small intestines of *μMT* CD-HFD mice (Figs. 3A, 3B). In addition, more IgM^{high}IgD^{high} and IgM^{low}IgD^{high} B cells were identified in WT CD-HFD compared to ND mice. As expected, μMT CD-HFD mice lacked B cells expressing IgM and/or IgD (Fig. 3C). More CD20^{+}MHC-II^{+} and CD20^{+}IgA^{+} B cells were found in WT CD-HFD compared to ND mice, whereas the latter were not increased in μM CD-HFD mice (Fig. 3D,E).

CD20^{+}IgA^{+}MHC-II^{+} cells were significantly elevated in WT CD-HFD small intestines (Fig. 3F), suggesting a potentially enhanced activation of these cells. CD20^{+}IgA^{+}CXCR4^{+} cells were also elevated in WT CD-HFD small intestines but were not detectable in *μMT* CD-HFD mice (Fig. 3G,H and Fig. S3A), indicating that B cells in small intestines of *μMT* mice most likely were not plasma blasts or plasma cells, since CXCR4 expression promotes the survival of long-term plasma cells.[32] Flow cytometry revealed more IgA^{+} and IgA^{+}B220^{-}CD20^{-} cells in WT CD-HFD small intestines, whereas, in *μMT* CD-HFD mice, this population remained at the same levels as in WT ND mice (Fig. 3I and Fig. S3B). IgA^{+}B220^{-}CD20^{-}CXCR4^{+} were significantly increased in WT CD-HFD but significantly less in *μMT* CD-HFD mice (Fig. 3J and Fig. S3C).

Cytometric t-distributed stochastic neighbour embedding (t-SNE) flow cytometry data analysis revealed a B-cell population diversity among the three investigated groups (Fig. 3K). We previously identified CD8^{+} T cells as important mediators of NASH and NASH-HCC(3, 4). Therefore, we investigated the

possible influence of intestinal B cells on this cell population. Flow cytometry analysis identified more $CD8^+$ T cells in *μMT* CD-HFD small intestines compared to WT CD-HFD and ND controls (Fig. S3F), and increased $CD8^+$ $CD44^+$ and $CD8^+$ $PD1^+$ cells were identified in WT and *μMT* CD-HFD small intestines (Fig. S3D, S3E). Moreover, cytometric t-SNE analysis showed diversity in the clustering of the $CD8^+$, $CD44^+$ and $PD1^+$ T-cell populations between the three groups (Fig. 3L).

3D high resolution of B–T-cell interactions in small intestines of WT ND and CD-HFD mice revealed $B220^+$ B cells co-localized with $CD8^+$ T cells. We observed significantly more interacting cell clusters (yellow) in WT CD-HFD intestines compared with ND controls (Fig. 3M and 3Q). Elevated $B220^+$ and $CD8^+$ cell interactions were also observed inside the villi of WT CD-HFD mice, suggesting a migratory phenotype of these cells (Fig. S3I, S3J). STRING[33] pathway enrichment and ImmuNET[34]bib34 analysis of functional relationship networks from RNA-sequencing data retrieved from $CD20^+$ and $B220^+$ sorted cells from WT ND, WT CD-HFD and μMT CD-HFD small intestines revealed enhanced expression of genes related to antigen presentation and BCR signalling, IgA production and B-cell activation and differentiation, and lipid metabolism (Figs. 3O, 3P and Fig. S3K,L), in both WT and *μMT* CD-HFD mice compared to ND controls.

To investigate whether intestinal B and T cells migrate from the gut to the liver during NASH, Kaede transgenic mice,[35] which constitutively express a photoconvertible fluorescent protein in all cells, were fed two different NASH diets, CD-HFD and western diet (WD) with trans-fat,[36] for 6 months. At 6 months, the gastrointestinal tissue of Kaede mice was photo-converted to label cells from green to red, enabling direct tracing of cells from the gastrointestinal tract to other tissues (Fig. 3R). Flow cytometry analyses of liver tissue revealed intestinal B cells migrating to the liver with fewer $B220^+$ $CD19^+$ $MHC\text{-}II^+$ B cells in the NASH-affected livers (red cells) compared to ND controls (Fig. 3S). Notably, liver $CD3^+$ cells migrating from the gut (red cells) were significantly increased compared with ND controls (Fig. 3S), suggesting that more T cells migrate from the gut to the liver during NASH.

We next aimed to assess if intestinal B cells derived from NASH-affected mice promote $CD8^+$ T-cell activation. To evaluate this, we co-cultured intestinal B cells from ND or CD-HFD mice with splenic $CD44^+$ $CD8^+$ T cells from ND mice and triggered TCR activation using anti-CD3/CD28 antibodies. $CD8^+$ T cells cultured with B cells from CD-HFD intestines exhibited significantly higher levels of the activation markers CD25 and CD69 than those cultured with B cells from ND mice after 24 h, which increased at 48 h. Likewise, these cells showed higher expression of the hallmarks of auto-aggressive T cells, namely CXCR6, PD1 and CTLA4, compared to T cells cultured with ND-derived B cells (Fig. 3T).

To investigate whether B cell-induced auto-aggression requires TCR-MHC-I or cell-cell interactions, we blocked MHC-I or LFA-1 and ICAM-1. Indeed, blockade of ICAM-1 or LFA-1 but not MHC-I abrogated B cell-induced T-cell activation *ex vivo* (Fig. 3T). To address whether observed B cell-induced T-cell activation is antigen-dependent, we used OT1 T cells harbouring transgenic TCR that recognizes only ovalbumin-derived antigens. OT1 T cells were activated by B cells derived from the gastrointestinal tract of NASH mice, supporting the notion of an antigen-independent metabolic activation (Fig. 3M). Collectively, these results indicate that in NASH conditions, intestinal B cells induce $CD8^+$ T-cell hyperactivation via ICAM-1 and LFA-1 but not TCR:MHC-I, indicating an antigen-independent activation mechanism.

These data suggest an altered metabolic and activated B-cell profile in the small intestine of NASH-affected mice. In addition, our data suggest that B cells from NASH-affected intestines cluster with $CD8^+$ T cells through direct cell-cell interaction, independent of an antigen but necessitating B-T cell interactions, which are stabilized via co-stimulatory molecules LFA-1 and ICAM1. Finally, our data indicate that intestinal B and T cells can efficiently migrate from the gut of NASH-affected mice to the liver.

IgA is sufficient to induce NASH in mice

To determine whether immunoglobulin secretion was required for NASH development, mice exhibiting normal B-cell development but lacking secreted immunoglobulin (*IgMi* mice[37,38]) were fed a CD-HFD for 6 months. We first tested whether these mice could develop normal immune responses, *e.g.* in a mouse model of multiple sclerosis. We found that the *IgMi* mice developed neurological impairment at a severity equivalent to WT when subjected to experimental allergic autoimmune encephalomyelitis (Fig. S4A), and *IgMi* T cells produced the same level of IL-2 as WT T cells when exposed to myelin oligodendrocyte glycoprotein peptide[39] (Fig. S4B). Thus, adaptive immune responses in these mice are largely intact. Despite similar development of obesity compared to WT CD-HFD mice, *IgMi* mice lacked signs of NASH upon CD-HFD (Fig 4A-C and Fig. S4C). Serum ALT and cholesterol, hepatic lipid deposition and hepatic triglycerides were significantly reduced in *IgMi* CD-HFD mice (Figs 4D,E and Fig. S4C). The number of $B220^+$ and $CD19^+$ cells remained unaltered (Fig. 4I and Fig. S4D), whereas $CD3^+$, $CD8^+$ $F4/80^{+,}$ and $MHC\text{-}II^+$ cells were significantly lower in IgMi CD-HFD livers (Fig. S4D, S4E). Moreover, $P62^+$ and cleaved caspase 3^+ cells were reduced in *IgMi* CD-HFD compared to WT CD-HFD mice (Fig. S4D). In addition, significantly fewer $CD8^+$, $CD8^+CD62L^+$, $CD8^+CD62L^-$ cells and $CD8^+TNF^+$ and $CD8^+IFN\gamma^+$ cells were observed in *IgMi* CD-HFD mice (Fig. 4F-H). Notably, flow cytometry analysis of the small intestine revealed the same increase in $CD20^+$, $CD20^+MHC\text{-}II^+$ and $CD8^+$ cells in IgMi and WT CD-HFD mice compared to controls, with *IgMi* mice demonstrating deficient levels of $CD20^+IgA^+$ cells,[37,38] as expected (Fig. 4L). Importantly, 3D high-resolution of immune cell interactions of B and T cells in the small intestine of WT ND, WT CD-HFD and *IgMi* CD-HFD mice (yellow) revealed a lack of interaction between $B220^+$ and $CD8^+$ cells in *IgMi* mice (Fig. 4J,K). The elevated $B220^+$ and $CD8^+$ interactions observed inside the villi of the WT CD-HFD intestines - when compared with ND controls - were not observed in the *IgMi* CD-HFD intestines (Fig. S4F). Astoundingly, IgMi mice displayed a reduction of phosphorylated SYK (a tyrosine-protein kinase mediating immune-cell activation pathways, such as BCR signalling) in immune cells of the small intestine, contrary to WT or *μMT* mice on CD-HFD (Fig. S4G).

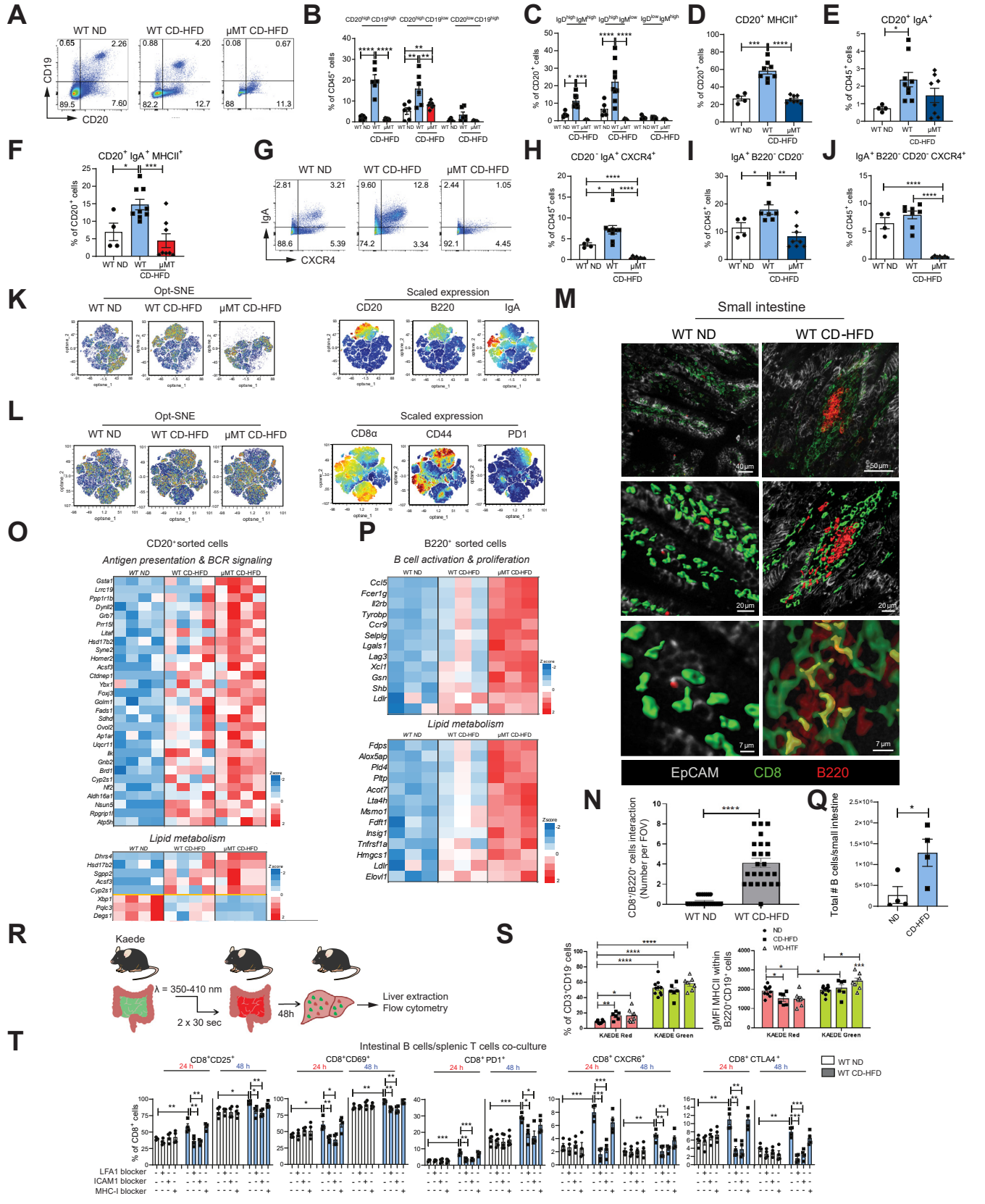

Fig. 3. B cells get metabolically activated and form clusters with T cells in the lamina propria of NASH-bearing mice. All data represent the small intestine. (A-J) Representative pseudocolor plots and quantifications of flow cytometric analyses comparing small intestine lamina propria from WT ND, WT CD-HFD and *μMT* CD-HFD male mice (≥4): (B) percentages of $CD20^+CD19^+$, $CD20^+CD19^-$, $CD20^-CD19^-$ cells, (C) IgD^+IgM^+, IgD^+IgM^-, IgD^-IgM^+ cells, (D) $CD20^+$MHC-II^+ cells, (E) $CD20^+IgA^+$ cells, (F) $CD20^+IgA^+$MHC-II^+ cells, (G) representative pseudocolor plots for IgA^+ and $CXCR4^+$ cells, (H) percentages of $CD20^-IgA^+CXCR4^+$ cells, (I) $IgA^+B220^-CD20^-$ cells, and (J) $IgA^+B220^-CD20^-CXCR4^+$ cells. (K) Automated optimized parameters for T-distributed stochastic neighbour embedding (opt-SNE) graphs from flow cytometric analysis of male mice (n = 9) displaying B cells. On the left, opt-SNE plots indicate scaled expression of CD20, B220 and IgA. (L) Opt-SNE graphs from flow

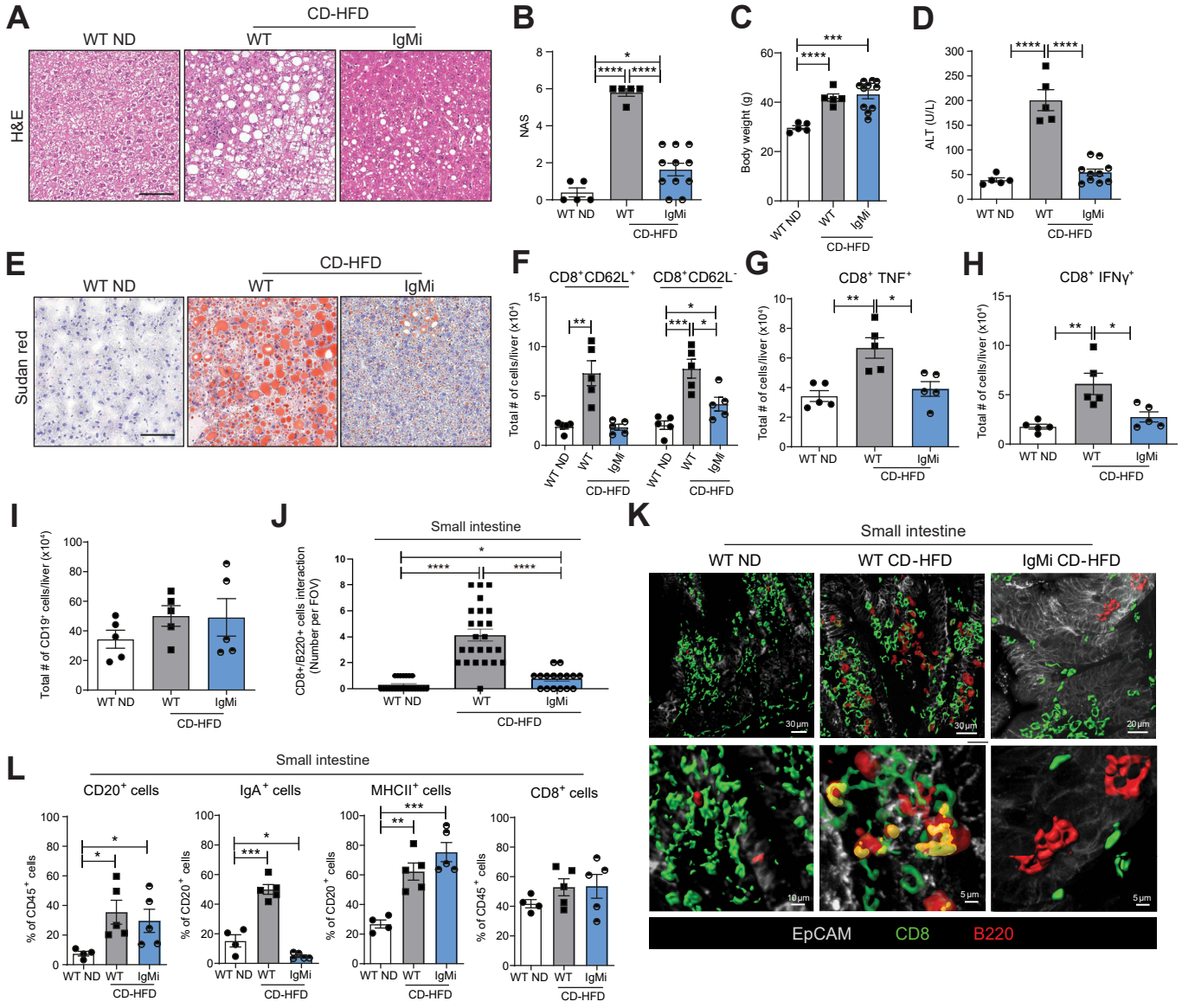

Fig. 4. Immunoglobulin secretion by B cells is essential for NASH development. (A) Representative H&E staining of liver sections from WT ND, WT CD-HFD and *IgMi* CD-HFD mice fed for 6 months. (B) NAS and (C) body weight measurement of male mice at 6 months post-diet-start (n ≥5). (D) Serological ALT male mice (n ≥5). (E) Representative Sudan red of liver sections. (F–I) Quantification of flow cytometry for (F) hepatic total CD8+CD62L+ and CD8+CD62L-cells, (G) total CD8+TNF+ cells, (H) total CD8+IFNγ+ cells, (I) total CD19+ cells, in male mice (n ≥4). (J) Quantification of hepatic clusters of B220+/CD8+ interacting cells in male mice (n = 3 for WT controls, n = 2 for IgMi CD-HFD mice, with n = 8 FOV each mouse). (K) Representative high-resolution confocal microscopy and 3D reconstruction images of small intestine lamina propria staining for B220+ cells and CD8+ cells (yellow areas indicate cell-cell contact between B220+ and CD8+ cells). (L) Quantification of flow cytometric analyses of small intestine CD20+, IgA+ cells, MHC-II+ cells, of CD8+ cells. All data are presented as mean ± SEM. Statistical analyses were performed using unpaired *t* test. Scale bars represent 100 µm, or as indicated.

cytometric analysis of male mice (n = 9) displaying T cells and scaled expression of CD8α, CD44 and PD1. (M) Representative high-resolution confocal microscopy and 3D reconstruction images of small intestine lamina propria staining for B220$^+$ and CD8$^+$ cells (yellow areas indicate a point of contact among B220$^+$ and CD8$^+$ cells), and (N) quantification of clusters of B220+/CD8+ interacting cells, (number cells interactions per field of view, FOV), in WT ND and WT CD-HFD (n = 3, with n = 8 FOV each mouse). (O, P) Heatmaps of immune system-related genes and metabolic process-related genes significantly different in small intestine lamina propria FACS-sorted (O) CD20$^+$ cells or (P) B220$^+$ cells isolated from WT and *µMT* CD-HFD *vs.* WT ND, indicated as z-scaled values. (Q) Flow cytometry quantification of total living B cells isolated from small intestine derived from male mice (6 months of diet) (n = 4). (R) Descriptive scheme for the flow cytometry performed with a transgenic mouse model of Kaede mice, bearing the photoconvertible fluorescence Kaede protein, which changes from green to red upon exposure to violet light: immune cells stained in red indicate migration into the liver from the small intestine; instead, cells stained in green are migrating immune cells from any other organ. (S) On the left, flow cytometric analysis indicates frequencies of liver CD3$^+$CD19$^-$ cells (n ≥5). On the right, geometrical MFI from flow cytometry analysis of Kaede red or green liver B220$^+$CD19$^+$ cells in ND, CD-HFD and WD-HTC mice (n ≥5). (T) Percentages of flow cytometry analysis of splenic CD8+CD69+, CD8+CD25+, CD8+PD1+, CD8+CXCR6+ and CD8+CTL4+ cells from CD44+CD8+ cells; splenic T cells isolated from a healthy mouse were stimulated with Dynabeads (anti-CD3/CD28) and were co-cultured for 24 or 48 h with intestinal B cells isolated from WT ND or WT CD-HFD. Additional treatments included Dynabeads plus LFA-1 blocker, or ICAM-1 blocker, or MHC-I blocker (n = 4). All data are presented as mean ± SEM. Statistical analyses were performed using unpaired *t* test.

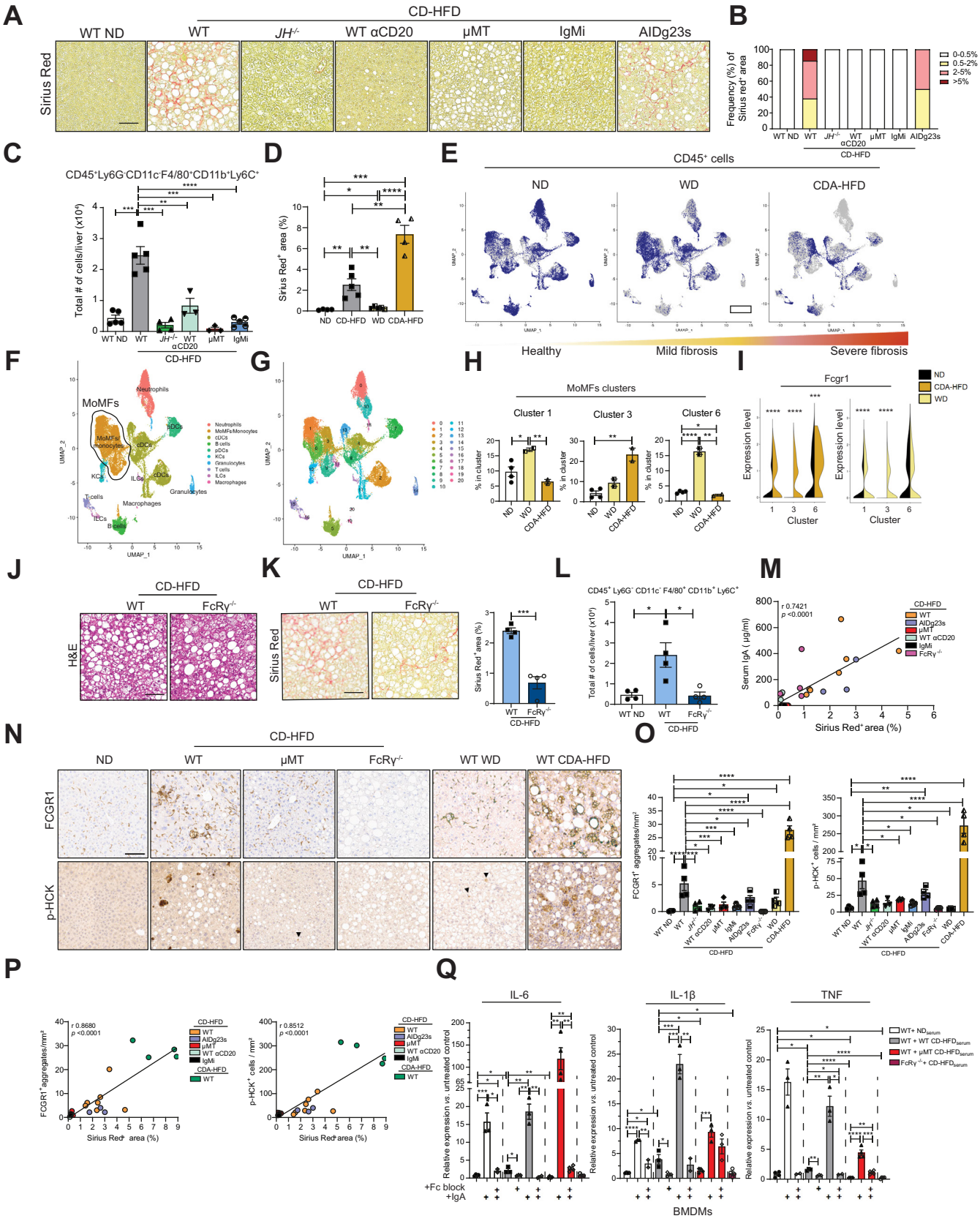

Fig. 5. FcR signalling activated in macrophages through IgA drives hepatic fibrosis in NASH. (A) Sirius red staining representative images from livers of WT ND and WT, *JH*$^{-/-}$, WT αCD20-treated, *μMT*, *IgMi*, *AIDg23s* mice (all under CD-HFD for 6 months). (B) Percentages of fibrosis incidence divided among the different degrees of fibrosis (mild 0.5-2%; moderate 2-5%; severe >5%) in above-mentioned mouse groups. (C) Quantifications of liver flow cytometric analyses of total CD45^{+}Ly6G^{-}Cd11c^{-}F4/80^{+}CD11b^{+}Ly6C^{+} cells from WT ND and WT, *JH*$^{-/-}$, WT αCD20-treated, *μMT*, *IgMi* mice under CD-HFD (n ≥3). (D) Sirius red quantification of

Overall, these observations suggest that secretion of IgA and IgM is important to support T-cell activation by metabolically activated B cells, with a crucial role in NASH induction. Intestinal membrane-bound IgA might affect the intensity and quality of B–T-cell interactions in the small intestine of NASH-affected mice.

NASH-induced fibrosis depends on IgA and Fc receptor signalling

NASH levels were the same in both WT and *μMT* CD-HFD mice, but tumour incidence was significantly lower in *μMT* mice (see Fig. 2). Therefore, we investigated fibrosis development in these mice as the latter could precede tumour development. In addition, we used another mouse strain termed *AIDg23s*[40] that exhibits reduced somatic hypermutation. From Sirius red, collagen IV and PDGFRβ staining on liver sections (Figs. 5A,B and Fig. S5A-C), transcriptional analyses of profibrogenic genes derived from livers of distinct mouse models (Fig. S5G) and serum hydroxyproline levels (Fig. S5H), fibrosis was solely found in WT and *AIDg23s* CD-HFD mice, but not in *JH*$^{-/-}$, *μMT*, *IgMi*, *IgA*$^{-/-}$[41] (lacking secreted IgA), *AID*$^{-/-}$[42] (lacking class switching) CD-HFD mice or in WT CD-HFD mice therapeutically treated with αCD20 antibody.

Having established a positive correlation between the presence of B cells and an intact immunoglobulin secretion function into the periphery (*e.g.*, IgA) with fibrosis (Fig. 5M and Fig. S5E,F), we sought to identify the hepatic immune cell compartment associated with NASH-related fibrosis (*e.g.*, in WT CD-HFD). Screening of several hepatic myeloid populations by flow cytometry identified CD45^{+}Ly6G^{-}CD11c^{-}F4/80^{+}CD11b^{+}Ly6C^{+} cells, classified as MoMFs,[21] in increased levels in the WT fibrotic NASH-affected mice (Fig. 5C). To determine whether MoMFs and NASH-induced fibrosis also correlate in other NASH models, we performed single-cell RNA-sequencing (scRNA-Seq) analyses of hepatic immune cell populations in also in WD and choline-deficient amino acid-specific high-fat diet (CDA-HFD)[43] models. The different NASH diets investigated represented a distinct spectrum of liver fibrosis severity (Figs. 5D and Fig. S5C). ScRNA-Seq analyses identified, among other immune cell populations, MoMFs to be associated in number and character with the degree of fibrosis (Fig. 5E,F and Fig. S5T). The MoMFs clusters 1, 3 and 6 were significantly increased in WD or CDA-HFD in the context of NASH-triggered fibrosis (Fig. 5G,H and Fig. S5U). The observed shift in the MoMF clusters depended on the diet mirroring the different degrees of fibrosis between the two diets (Fig. S5S). Notably, MoMFs – but not other immune cell populations – strongly upregulated FcR-genes and genes involved in FcR signalling activation in all NASH diets, including increased transcription of *Fcgr1,* and *Fos* genes, especially in MoMFs derived from the severe fibrotic mouse group CDA-HFD (Fig. 5I and Fig. S5U). This observation was corroborated by protein expression by FCGR1 IHC on liver sections (Fig. 5N, 5O).

FcγR activation induces macrophage phagocytosis.[44] During infection, these processes are controlled by IgA molecules surrounding infectious antigens. These complexes are recognized mainly by FcαR (CD89) in human macrophages[45] and by FcγRI (FCGR1), FcγRIIIa (FCGR3) and FcεRI (FCER1G) in mice, all having in common the intramembrane portion of FcγR for downstream signalling activation.[46] The degree of fibrosis correlated with serological IgA levels in the NASH models analysed, suggesting a link between immunoglobulin levels and Fc receptor activation. To functionally evaluate whether the absence of FcγR expression, which inhibits functional FCGR1, FCGR3 and FCER1G activity, could reduce macrophage activation and fibrosis in NASH, *FcRγ*$^{-/-}$ mice were fed a CD-HFD for 6 months. Although these mice developed full-blown NASH, steatosis, liver damage (Figs. 5J and Fig. S5I, S5J), and a similar liver inflammatory profile compared to WT controls (Fig. S5K,L), *FcRγ*$^{-/-}$ mice displayed strongly reduced fibrosis (Fig. 5K) that correlated positively with reduced serum IgA levels and the number of hepatic MoMFs (Figs. 5L and Fig. S5M). As expected, *FcRγ*$^{-/-}$ mice lacked FCRG1 expression and FcR-downstream signalling, as determined by reduced phosphorylated HCK, a downstream mediator of FcR signalling, compared to mice with fibrosis (Figs. 5N-5P).

To determine whether the observed *in vivo* phenotype in *FcRγ*$^{-/-}$ mice fed a CD-HFD relied primarily on the lack of FcRg-signalling rather than altered myeloid-cell trafficking, we evaluated the migration capability of *FcRγ*$^{+/+}$ and *FcRγ*$^{-/-}$ myeloid cells *in vivo* and *in vitro*. Bone marrow-derived macrophages (BMDMs) from *FcRγ*$^{-/-}$ and control mice, previously injected with carbon tetrachloride short-term, were analysed for their migration capacity (Fig. S5P). A CCL2 gradient induced similar transmigration efficacy of *FcRγ*$^{+/+}$ and *FcRγ*$^{-/-}$ BMDMs, as investigated by transmigration assays and subsequent flow cytometry (Fig. S5Q). In the livers of carbon tetrachloride-treated mice, hepatic MoMFs were similarly increased in both

livers from 4-month WT ND, WT CD-HFD, WT WD-HTF or CDA-HFD (n ≥4). (E) CD45^{+} cells from livers of 4-month ND, WD-HTF and CDA-HFD (all WT) fed mice were sorted and 10X single-cell RNA-seq experiments were performed (n ≥2); Representative UMAP plots visualizing single-cell RNA-sequenced CD45^{+} cells from livers of 4-month ND, WD-HTF and CDA-HFD, indicating individual cell spatial positions in blue colour among the three groups. (F) UMAP plot visualizing immune cell populations FACS-sorted by CD45^{+}. The identified immune cells population displayed are MoMFs/monocytes, KCs, DCs, neutrophils, T cells, B cells, plasma B cells, diving cells, NKT cells, and ILCs. (G) UMAP plot visualizing cell clusters of single-cell RNA-sequenced CD45^{+} cells of all mouse groups (legend reporting the number of cells in parentheses). (H) Abundance plots showing relative percentages of MoMF clusters majorly differentiated under diet-experimental conditions[1,3,6] of 4-month ND, WD-HTF and CDA-HFD mice (n ≥2). (I) Double-violin plots showing the mRNA expression of *Fcgr1* in most relevant MoMF clusters, comparing CDA-HFD or WD against ND mice (n ≥2). (J) Representative H&E staining of liver sections of 6-month WT and *FcRγ*$^{-/-}$ male mice fed with CD-HFD. (K) Representative Sirius red staining and quantification of liver sections of 6-month WT and *FcRγ*$^{-/-}$ male mice fed with CD-HFD (n = 4). (L) Quantifications of liver flow cytometric analyses of total CD45^{+}Ly6G^{-}Cd11c^{-}F4/80^{+}CD11b^{+}Ly6C^{+} cells in WT and *FcRγ*$^{-/-}$ male mice fed with CD-HFD (n = 4). (M) Correlation plot indicating serological IgA and Sirius red positivity in CD-HFD male mice (n ≥3). (N) Representative IHC images of FCGR1 staining of liver sections and (O) quantifications of FCGR1^{+} aggregates per mm^{2} (n ≥3) and phospho-HCK (per mm^{2}) (n ≥3). (P) Correlation plots indicating FCGR1^{+} aggregates per mm^{2} and Sirius red positivity, and p-HCK^{+} cells per mm^{2} and Sirius red positivity (n ≥3). (Q) Relative mRNA expression levels measured through qRT-PCR of major profibrogenic genes from 12-weeks in WT or *FcRγ*$^{-/-}$ BMDMs, after stimulation with serum of WT ND, WT CD-HFD or μMT CD-HFD (6-months under diet) (n ≥2), with or without the addition of IgA alone or in combination with Fc-blocker. Complement proteins were deactivated with a serum pre-treatment of 30 min at 56 °C. All data are presented as mean ± SEM. Statistical analyses were performed using unpaired *t* test or Pearson correlation's test. The scale bar represents 100 μm.

A

Exp. mouse group	B cells & immunoglobulins	NASH	Hepatic fibrosis	B-T cells gut interaction	HCC
WT CD-HFD	LP & SLOs, B cells, IgA, IgM, IgG	Yes	Yes	Yes	Yes (~30%)
JH$^{-/-}$ CD-HFD	No	No	No	-	No
μMT CD-HFD	only LP IgA B cells	Yes	No	-	low incidence (5%)
αCD20 WT CD-HFD	only long-lived plasma cells	No	No	-	-
IgA$^{-/-}$ CD-HFD	low afinity IgM	Yes	No	-	-
AID$^{-/-}$ CD-HFD	low afinity IgM	Yes	No	-	-
AIDg23s CD-HFD	low affinity IgM & IgA	Yes	Yes	-	-
IgMi CD-HFD	No secreted IgM & IgA, only IgG	No	No	No	-
FcRγ$^{-/-}$ CD-HFD	B cells and immunoglobulin secretion not affected	Yes	No	-	-
Germ Free (GF) CD-HFD	B cells and immunoglobulin secretion not affected	Yes	Yes	Yes	-
αCD20 GF WT CD-HFD	only long-lived plasma cells	No	No	-	-

- = Not tested

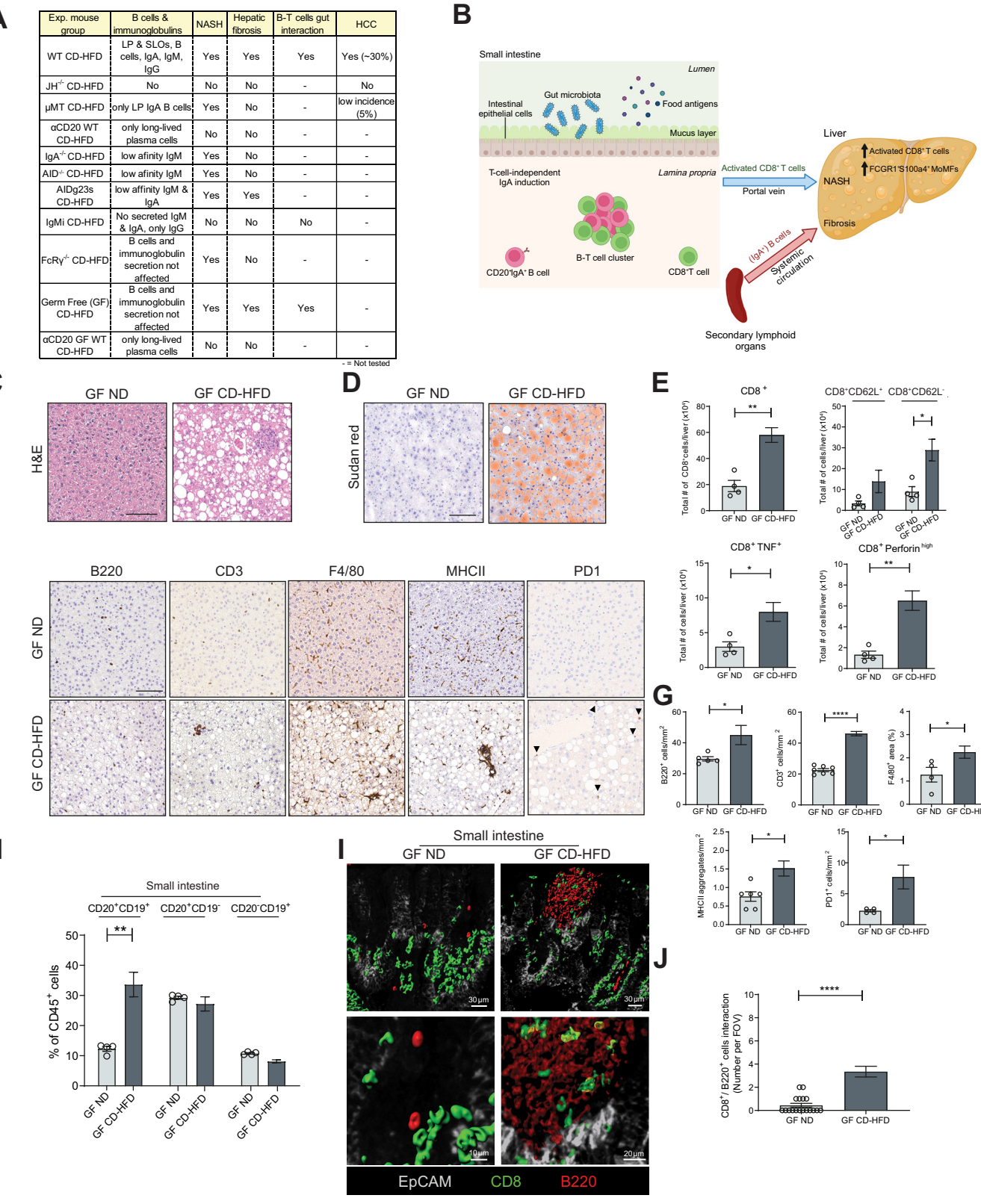

Fig. 6. Summary of models, including germ-free mice on NASH diet. (A) Table indicating NASH phenotypes, B cells/immunoglobulin types, fibrosis, B-T cell interactions and HCC in all mouse models applied in this study research. (B) Graphical summary displaying the role of lamina propria CD20$^+$IgA$^+$B cells in the context of NASH activated externally to lymphoid follicles and increased in number, forming clusters with CD8$^+$ T cells. The latter may migrate from the lamina propria to the liver via the portal vein. Secondary lymphoid organ (*e.g.*, spleen) derived IgA$^+$B cells contribute via IgA$^+$ to liver fibrosis through activation of FcRγ signalling in monocyte-derived macrophages (positive for FCGR1, S100a4, Ly6C, CD11b, F4/80). (C) Representative H&E staining of liver sections derived from GF WT ND and GF WT CD-HFD male mice fed for 6 months. (D) Representative Sudan red staining of liver sections from GF male mice (CD-HFD for 6 months). (E) Quantifications of liver flow

mouse groups compared to their untreated counterpart (Fig. S5R). Next, levels of general MoMF markers Ly6C and the profibrogenic macrophage marker S100A4 were assessed in several mouse models fed a NASH diet. Increased Ly6C$^+$ cells were found in those mice that displayed fibrosis – WT and *AIDg23s* CD-HFD mice – but not in other mouse models on CD-HFD (Fig. S5N).[47] Quantification of hepatic Ly6C$^+$/CD11b$^+$/FCER1G$^+$ cells of WT ND, and WT, *μMT*, WT αCD20, *IgMi* and *AIDg23s* mice – all on CD-HFD – showed that fibrotic livers such as WT and AIDg23s CD-HFD display a significantly higher amount of Ly6C$^+$/CD11b$^+$/FCER1G$^+$ cells (Fig. S6V,W).

A possible role for IgA and FcRγ-signalling in activating profibrogenic macrophages was investigated by measuring the expression of selected profibrogenic/activation genes such as IL-1β, IL-6 and TNF by BMDMs *ex vivo*. BMDMs from 12-week-old WT or *FcRγ*$^{-/-}$ mice were first treated *in vitro* with serum derived from healthy WT ND or fibrotic WT CD-HFD mice (both 6 months on diet) (Fig. S5O). Serum from fibrotic WT CD-HFD induced increased expression of the profibrogenic genes compared to ND serum (Fig. 5Q). WT-BMDMs treated with serum from μMT CD-HFD mice, which have NASH but are devoid of systemic IgA secretion and fibrosis, failed to induce profibrogenic/activation genes (Fig. 5Q). In contrast, the addition of purified IgA added to serum derived from WT ND or *μMT* CD-HFD mice strongly induced the expression of IL-6, IL-1β and TNF in BMDMs, which was abrogated by addition of an Fc-blocker (Fig. 5Q). Strikingly, the addition of Fc-blocker to serum derived from fibrotic WT CD-HFD mice prevented the induction of IL-6, IL-1β and TNF in BMDMs (Fig. 5Q). These data indicate that immunoglobulins (*e.g.*, IgA) circulating in serum from NASH mice may directly trigger BMDM-activation. As an additional control, *FcRγ*$^{-/-}$-BMDMs were treated with the serum of fibrotic CD-HFD mice, which failed to induce the expression of IL-6, IL-1β and TNF in BMBMs, again highlighting that FcRγ-signalling is involved in immunoglobulin-mediated transduction processes (Fig. 5Q).

Overall, these data indicate that FcRγ-signalling, mainly in MoMFs, plays an important role in the development of hepatic fibrosis in NASH and that secreted immunoglobulin is a critical factor in activating this signalling.

Fig. 6A summarizes the most important data presented so far. We propose that B cells can act via two mechanisms: (i) an extrafollicular, intestinal mechanism that can promote activation and transmigration of T cells in the liver and (ii) a mechanism involving the secretion of immunoglobulins, most likely IgA, that can drive the activation of MoMFs in the liver and promote the initiation of fibrosis (Fig. 6B).

The gut microbiota is not necessary for NASH development

The gut microbiota has an important role in the homeostasis of gut B cells.[48,49] So far, studies have suggested that germ-free (GF) mice were resistant to obesity[50] depending on the type of diet,[51,52] and NAFLD/NASH development.[53–55] However, GF mice fed a WD for 16 weeks developed obesity and demonstrated metabolic dysfunction,[56] indicating that the absence of microbiota might allow for the development of metabolic syndrome.

To investigate this concept in the context of NASH and the related B-cell functions, GF mice were fed a CD-HFD for 6 months. CD-HFD mice gained significant weight (Fig. S6A) and displayed full-blown NASH and impaired glucose response (Fig. 6C,D and Fig. S6A,B,G), more hepatic T cells, B cells and activated CD8$^+$ T cells expressing TNF and Perforin (Fig. 6E), and F4/80$^+$ cells and MHC-II$^+$ aggregates (Fig. 6F,G). In the small intestine, CD-HFD mice presented increased B-cell frequencies (Fig. 6H), and also showed B220$^+$/CD8$^+$ cells forming clusters (yellow), especially along intestinal villi (Fig. 6I,J).

The importance of B cells for NASH development under GF conditions was tested by administering an αCD20 antibody for 6 weeks, starting at month 4 on CD-HFD – a time-point by which mice on a CD-HFD have already developed NASH and liver damage (Fig. S6D,E). B-cell depletion efficacy was proven effective in different tissues (spleen, liver and small intestine) (Fig. S6K).

Anti-CD20 antibody-treated GF CD-HFD mice were obese and rescued for NASH but not for steatosis and showed unchanged serum ALT and cholesterol levels (Figs. S6G-J). Furthermore, αCD20 antibody-treated GF CD-HFD livers were not inflamed and showed significantly fewer activated CD8$^+$ T and F4/80$^+$ cells (Fig. S6K,L), whereas MHC-II$^+$ aggregates remained on the same levels compared to untreated controls (Fig. S6L).

These data suggest that the gut microbiota was not necessary to induce obesity and NASH, proposing a sterile metabolic activation of immune cells to be sufficient to drive NASH(3, 4, 29). Moreover, B cells could act independently of the gut microbiota to contribute to NASH development and interact with the T cells in the small intestine.

Increased gastrointestinal CD20$^+$ B cells, high IgA levels and FcRγ$^+$ myeloid cells in patients with NASH and cirrhosis

Next, we compared the data obtained from our mouse NASH models in patients with NASH. Similar to our mouse NASH models, an increase of CD20$^+$ B cells was found in gastrointestinal tissue (*e.g.*, jejunum) taken during bariatric surgery from patients with NASH when compared to patients with simple steatosis (Fig. 7A,B). Moreover, we found increased phosphorylated SYK$^+$ in jejunal immune cells (including CD20$^+$ B cells) of patients with NASH *vs*. simple steatosis (Fig. 7C, and Fig. S7A,J), indicative of B-cell activation.

We could corroborate previously published data demonstrating elevated serum IgA levels positively correlating with the degree of fibrosis in two distinct patient cohorts (Fig. 7D,E and Fig. S2B).[22] Moreover, increased levels of IgA significantly correlated with the presence of portal inflammation (Fig. 7F,G).

cytometric analyses comparing 6-month GF ND, and GF CD-HFD for total CD8$^+$ cells, CD8$^+$CD62L$^+$ and CD8$^+$CD62L$^-$ cells, CD8$^+$TNF$^+$ cells, and CD8$^+$perforin^{high} cells (n = 4). (F) Representative IHC images of liver sections and (G) quantifications per mm^2 for B220, CD3, F4/80 and MHC-II staining of GF ND and GF CD-HFD mice (n = 5). (H) Quantifications of small intestine flow cytometric analyses of CD20$^+$CD19$^+$, CD20$^+$CD19$^-$ and CD20$^-$CD19$^+$ cells in GF male mice (n = 4). (I) Representative high-resolution confocal microscopy and 3D reconstruction images of small intestine lamina propria staining for B220+ and CD8+ cells (yellow areas indicate a point of contact among B220+ and CD8+ cells), and (J) quantification of clusters of B220+/CD8+ interacting cells, of GF male mice (n = 3, with n ≥4 FOV each mouse). All data are presented as mean ± SEM. Statistical analyses were performed using unpaired *t* test. The scale bar represents 100 μm.

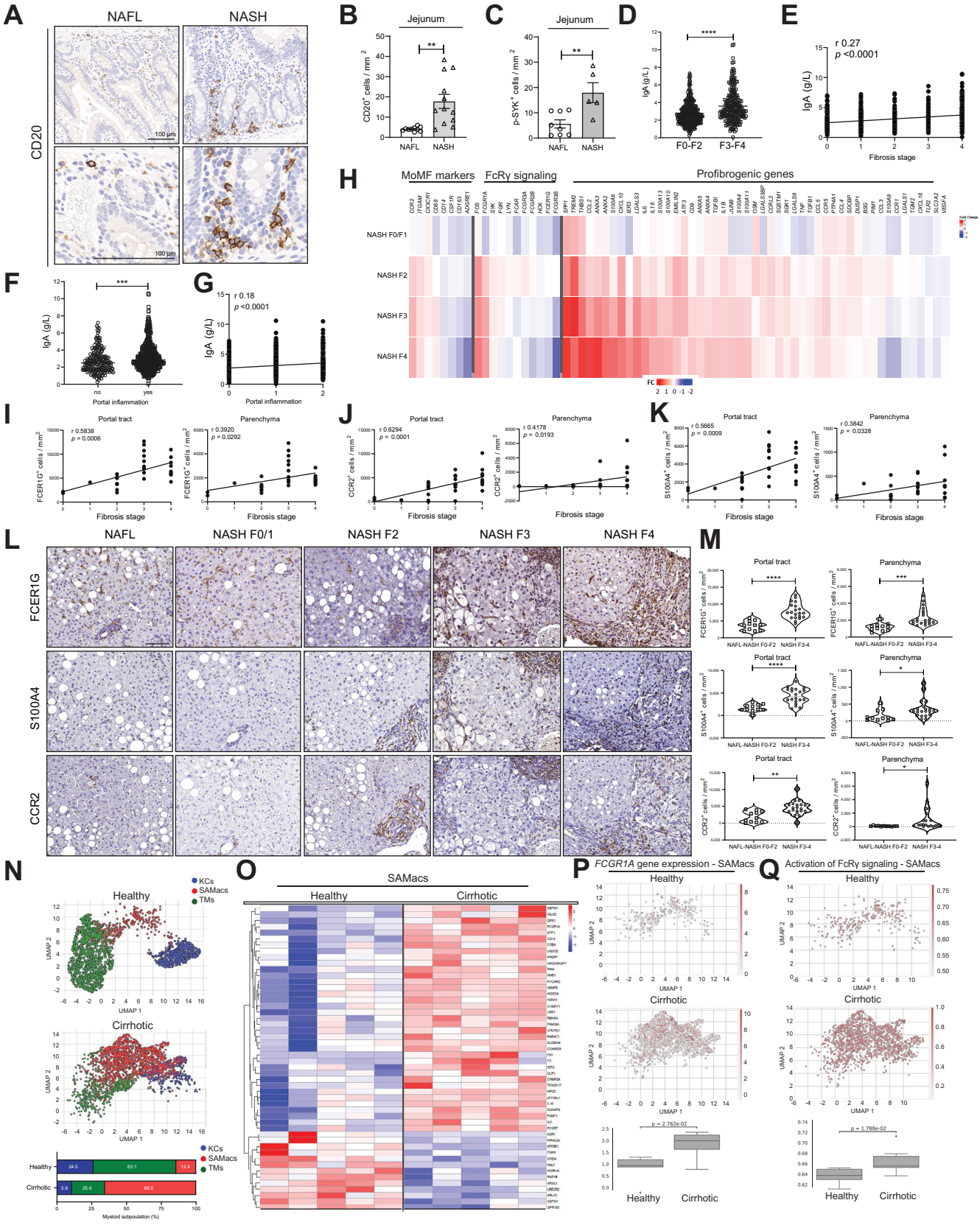

Fig. 7. Intestinal B cells and hepatic myeloid cells in NAFLD-affected patients. (A) Representative CD20 stained jejunum samples of NAFL and NASH-affected patients. (B) CD20^{+} cells quantification in jejuna of patients with NAFL, and NASH, per mm^{2} (n ≥4). (C) Phospho-SYK quantification on immune cells (B cells or myeloid cells) in jejuna on patients with NAFL or NASH (n ≥5). (D) Serum measurement of IgA levels in patients with NAFLD divided into two subgroups (F0–F2 and F3–F4) based on fibrosis score (Brunt/Kleiner scoring) (n ≥233 each group, total n = 639). (E) Correlation plot of IgA serological levels and fibrosis stage in NAFLD patient

Notably, IgG but not IgM levels were elevated in higher fibrosis stages (Fig. S7B). Interestingly, patients with NAFLD and rheumatoid arthritis – treated with a monoclonal αCD20 antibody – displayed reduced serum ALT levels (Fig. S7E), supporting the notion that B-cell depletion might ameliorate liver damage in patients with NASH. High levels of serum IgA were associated with parenchymal and portal tract $PD1^+$ cells but not with $CD8^+$ T cells in patients with NASH, indicating a possible link between IgA secretion, fibrosis, and $PD1^+$ cells (Fig. S7F,G).

Our mouse data presented above suggested that MoMFs correlated strongly with fibrogenesis.[57,58] In a large NAFLD cohort of patients with different degrees of fibrosis, we performed a total liver transcriptomic analysis of selected genes for MoMFs, FcRγ signalling and fibrogenesis. We found that many relevant genes of these categories, including *CCR2*, *ITGAM*, *CX_3CR1* (indicative of MoMFs phenotype), *FOS* and *FCGR1A* (FcRγ-signalling), *SPP1*, *TREM2*, *THBS1*, *CCL2*, and S100A4 among other profibrogenic genes were directly correlated with the degree of fibrosis (Fig. 7H), similar to our mouse analysis. We also found a strong correlation between the chemokine receptor *CCR2* and *S100A* with *FCER1G* at a transcriptomic level (Fig. S7H).

In human NAFLD livers, the number of $FCER1G^+$, $CCR2^+$ and $S100A4^+$ cells in the portal tract and parenchyma correlated with the degree of fibrosis (Fig. 7I-7K). Mainly, fibrotic areas were densely populated with infiltrating $S100A4^+FCER1G^+CCR2^+$ cells and stratification of patients with NAFLD based on the fibrosis stage showed a significant increase in advanced NAFLD (Fig. 7L,M, and S7H,I). In contrast, no difference was observed in the density of $CD163^+FCER1G^+$ cells among different fibrotic stages, indicating a marginal role of Kupffer cells in fibrosis (data not shown).

Further, we analysed whether myeloid-cell populations driving fibrosis and/or cirrhosis would be activated by similar pathways to those identified in our mouse NASH models. ScRNA-Seq analysis of $CD45^+$ cells derived from healthy liver tissue (transplantation donors) and NAFLD-cirrhotic livers showed that patients with cirrhosis displayed an increased compartment of a subpopulation of myeloid cells called scar-associated macrophages (SAMs) (Fig. 7N,O and S7K).[59] Notably, we found that *FCGR1A* gene expression was significantly increased in patients with cirrhosis compared with healthy donors (Fig. 7P) and that the FcRγ-signalling signature was significantly increased in patients with cirrhosis compared with healthy donors, being particularly enriched in the SAM compartment (Fig. 7Q). Transcriptional analyses and comparison of FcRγ-signalling pathways in mouse and human NASH livers revealed close similarities in the regulation of the FcRγ-signalling components as well as downstream targets (Fig. S7L).

In summary, data from patients with NASH suggest an important role for secreted IgA and FcRγ-signalling on MoMFs/SAMs in the development of fibrosis and/or cirrhosis, in agreement with the data derived from NASH mouse models.

Discussion

Herein, we describe two distinct B cell-dependent mechanisms that promote (i) metabolic T-cell activation in the gastrointestinal tract and (ii) aggravate liver fibrosis in NASH (Fig. 6A,B). We have previously shown that auto-aggressive T cells exacerbate progressive liver disease in NASH, leading to HCC development.[3,4] We report that T-cell activation, hepatic inflammation, NASH, fibrosis and liver tumorigenesis were abrogated *in vivo* by genetic depletion of B cells ($JH^{-/-}$ mice). Therapeutic depletion of B cells in mice with NASH/fibrosis led to a reduction/reversal of T-cell-driven inflammation and fibrosis. ^{1}H-NMR and mass-spectrometry analyses demonstrated that B cells contribute to hepatic metabolic alterations that characterise NASH pathophysiology.

As the gut-liver axis has been identified as a critical factor in NAFLD pathophysiology,[14] we assessed the role of gastrointestinal B cells (*μMT* mice). This assessment revealed that gastrointestinal IgA^+ B cells contribute to T cell–driven inflammation and metabolic alterations in the liver but cannot drive fibrosis owing to their inability to secrete immunoglobulins into the periphery. These gastrointestinal B cells developed in the lamina propria in a T cell-independent manner,[60] albeit at low numbers, were strongly activated in the context of NASH. NASH-driven HCC incidence was significantly lower in *μMT* mice despite exhibiting equivalent quality and levels of NASH compared to WT CD-HFD, potentially attributable to the absence of hepatic fibrosis in *μMT* CD-HFD mice. Therapeutic depletion of gastrointestinal B cells in *μMT* mice reduced T-cell inflammation *in vivo* and reverted NASH.

Further analysis in WT mice on a NASH diet showed that gastrointestinal B cells were elevated in number, metabolically activated and displayed activated BCR signalling. When we analysed human intestinal tissue from patients with NASH, we also observed an increase in B-cell number compared to unaffected patients or patients with simple steatosis.

In the lamina propria of the small intestine of NASH mice, B cells and $CD8^+$ T cells formed clusters with cell-cell interactions, suggesting that within these clusters, B cells could activate $CD8^+$ T cells. However, these clusters were not found

cohort of 639 individuals. (F) Serum measurement of IgA levels in patients with NAFLD divided into two subgroups based on the absence or presence of liver portal inflammation (n ≥233 each group, total n = 639). (G) Correlation plot of IgA serological levels and portal inflammation scores in the NAFLD patient cohort of 639 individuals. (H) Heatmaps showing transcriptomics analysis derived $\log_2$ fold-change values of selected genes involved in the monocyte-derived macrophage phenotype, in FcRγ signalling and in fibrogenesis, from patients with NAFLD and with different degrees of fibrosis *vs.* patients with NAFL (total n = 206). (I–K) Correlation plots of fibrosis stage and portal tract or parenchymal (I) $FCER1G^+$ cells/mm^2, (J) $CCR2^+$ cells/mm^2, or (K) $S10014^+$ cells/mm^2 (n = 31). (L) IHC representative images of FCER1G, CCR2 and S100A4 in patients with NAFLD, with absent/very low fibrosis (F0/F1) and high fibrosis (F3), and their quantifications (M) in two fibrosis subgroups for portal and parenchymal quantified stained cells (n ≥11). (N) UMAP plots indicating liver $CD45^+$ FACS-sorted cells and subsequently single-cell 10X RNA-sequenced, divided into TMs, KCs, and SAMs, from healthy donors and patients with NAFLD-related cirrhosis, and percentages of each myeloid subpopulation below (n ≥5). (O) Heatmaps indicating the top 100 most variable genes among healthy donors and patients with cirrhosis in SAMac population (n = 5). (P) UMAP plots indicating mRNA expression scores of *FCGR1A* gene in SAMs from healthy donors and patients with NAFLD and cirrhosis, with statistical analysis below (n ≥5). (Q) Expression scores of activated FcRγ signature (Reactome) in healthy donor livers and in NAFLD/ALD-cirrhotic SAM population, with statistical analysis below (n ≥5). All data are presented as mean ± SEM. Statistical analyses were performed using unpaired *t* test or Pearson correlation's test.. The scale bar for IHC represents 100 μm, for immunofluorescence 50 μm.

in ND-fed mice. Our data indicate that hyperactivation of $CD8^+$ T cells by the gastrointestinal B cells in NASH is achieved via a licensing step that requires direct cell-cell interaction.

Importantly, we could demonstrate that B cells derived from small intestines of NASH mice can directly activate $CD8^+$ T cells *ex vivo* in an antigen-specific independent manner, necessitating LFA-1 and ICAM-1 but not MHC-I. In contrast, intestinal B cells from ND-fed mice could not activate T cells *ex vivo*. Our data indicate that auto-aggression and hyperactivation of $CD8^+$ T cells via the gastrointestinal B cells in NASH is achieved by a licensing step that requires direct cell-cell interaction. Interference with the LFA1-ICAM axis abrogated T-cell hyperactivation *ex vivo*. Moreover, activation of $CD8^+$ T cells was TCR-independent – as gastrointestinal B cells also activated OT1-CD8+ T cells. Interaction of $CD8^+$ T cells with the gastrointestinal B cells acts as an amplifier of downstream TCR signalling without the involvement of antigen-specific presentation by B cells, as blockade of MHC-I did not prevent B cell-induced auto-aggression.

Besides metabolic re-programming, activated NASH gastrointestinal B cells or amplified BCR signalling are potentially represented by phosphorylation of SYK[61-64]. The latter was absent in the B cells of IgMi mice, which are protected from NASH and lack B-T cell clusters in the small intestine. Notably, in hyperactivated B cells, as in the case of lymphoma, SYK inhibitors are exploited therapeutically.[65]

Using Kaede mice and their capability to photoactivate cells locally, we enabled tracking of B and T cells from the gastrointestinal tract to the liver in the context of NASH. We suggest that metabolically activated gastrointestinal B and T cells migrate from the gut to the liver, indicating that metabolically activated T cells may originate in the small intestine, migrate to and potentially be maintained in the liver.

Given the central role of gastrointestinal B cells in NASH development, we proceeded to study the role of microbiota[15–17] in our disease models. We showed that NASH development occurred without the gut microbiota in a NASH diet model (CD-HFD). Therapeutic depletion of B cells in GF mice with NASH reversed liver inflammation and fibrosis, indicating that B cells lead to T-cell activation and NASH - independently of the gut microbiota.

It has been shown that serum IgA levels were elevated in patients with NAFLD(22). Our *in vivo* and *in vitro* NASH studies demonstrated that secretion of IgA contributed to fibrosis by activating FcRγ-signalling in $CD11b^+CCR2^+F4/80^+CD11c^-FCGR1^+$ MoMFs.[66] However, we cannot exclude that other cell types expressing Fc receptors (*e.g.*, hepatocytes) may also contribute to this phenotype. Notably, in molecular analysis of patients with NASH, serum IgA levels correlated with fibrosis severity and with FcRγ-activated SAMs in the liver.

Thus, besides other known immune cell mechanisms that drive NASH and fibrosis,[67] B cells and IgA secretion are clearly important players in the pathogenesis of NAFLD/fibrosis/cirrhosis. It will be interesting to decipher further the role of B cells in hepatic lipid accumulation and metabolic dysregulation. New therapeutic approaches in NASH suggest combination therapies with anti-steatosis, anti-inflammatory, and anti-fibrotic drugs may be effective.[68]

Our study shows that gastrointestinal B cells are a potential target for such a combinatorial therapeutic approach, as we have identified them as mediators of licensing metabolic T-cell activation and fibrosis. Future studies blocking the interaction between B and T cells, specifically in the gut, and targeting FcR signalling in the liver, might illuminate new therapeutic avenues against NASH and NASH-related fibrosis.

Affiliations

[1]Division of Chronic Inflammation and Cancer, German Cancer Research Center Heidelberg (DKFZ), Heidelberg, Germany; [2]Research Unit of Radiation Cytogenetics (ZYTO), Helmholtz Zentrum München, Neuherberg, Germany; [3]Institute of Molecular Oncology and Functional Genomics, Clinic and Polyclinic for Internal Medicine II, Klinikum rechts der Isar of the Technical University of Munich (TUM), Munich, Germany; [4]Translational and Clinical Research Institute, Faculty of Medical Sciences, Newcastle University, Newcastle, UK; [5]Maurice Müller Laboratories (DBMR), University Department of Visceral Surgery and Medicine Inselspital, University of Bern, Bern, Switzerland; [6]Institute of Molecular Medicine and Experimental Immunology, University Hospital, Bonn, Germany; [7]Nutrition and Immunology, Technical University of Munich, Freising-Weihenstephan, Germany; [8]ZIEL - Institute for Food and Health, Technical University of Munich, Freising-Weihenstephan, Germany; [9]Department of Hepatology and Gastroenterology, Charité Universitätsmedizin Berlin, Campus Virchow-Klinikum and Campus Charité Mitte, Berlin, Germany; [10]Division of Vascular Oncology and Metastasis, German Cancer Research Center Heidelberg (DKFZ-ZMBH Alliance), Heidelberg, Germany; [11]European Center of Angioscience (ECAS), Medical Faculty Mannheim, Heidelberg University, Mannheim, Germany; [12]Department of Preclinical Imaging and Radiopharmacy, Werner Siemens Imaging Center (WSIC), Tübingen University, Tübingen, Germany; [13]The Concern Foundation Laboratories at the Lautenberg Center for Immunology and Cancer Research, IMRIC, Faculty of Medicine, Hebrew University-Hadassah Medical School, Jerusalem, Israel; [14]Internal Medicine I, University Hospital Tübingen, Faculty of Medicine, University of Tübingen, Tübingen, Germany; [15]Department of Computer Science, University of Tübingen, Tübingen, Germany; [16]Section of Molecular Immunology und Gastroenterology, I. Department of Medicine, University Medical Center Hamburg-Eppendorf, Hamburg, Germany; [17]Department of Medicine II, University Hospital Freiburg - Faculty of Medicine, University of Freiburg, Freiburg, Germany; [18]Center for Translational Cancer Research (TranslaTUM), Technical University of Munich (TUM), Munich, Germany; [19]Department of General, Visceral and Transplantation Surgery, University of Heidelberg, Heidelberg, Germany; [20]Research Center for Immunotherapy (FZI), University Medical Center at the Johannes Gutenberg University, Mainz, Germany; [21]Institute for Molecular Medicine, University Medical Center of the Johannes Gutenberg University, Mainz, Germany; [22]Division of Hepatology, University-Hospital Würzburg, Würzburg, Germany; [23]Rheumatology/Clinical Immunology, Kreiskliniken Altötting-Burghausen, Burghausen, Germany; [24]Rheumatology, Medical Clinic II, Julius-Maximilians-University Würzburg, Germany; [25]Centre for Inflammation Research, The Queen's Medical Research Institute, University of Edinburgh, Edinburgh, UK; [26]MRC Human Genetics Unit, Institute of Genetics and Molecular Medicine, University of Edinburgh, Edinburgh, UK; [27]Department of Immunobiology, Yale University School of Medicine, New Haven, USA; [28]Institute of Pathology, Technical University of Munich (TUM), Munich, Germany; [29]Comparative Experimental Pathology, Technical University of Munich (TUM), Munich, Germany; [30]Division of Chromatin Networks, German Cancer Research Center (DKFZ) and Bioquant, Heidelberg, Germany; [31]Department of Pathology and Molecular Pathology, University and University Hospital Zurich, Zurich, Switzerland; [32]Department Internal Medicine I, Eberhard-Karls University, Tübingen, Germany; [33]Department of Gastroenterology, Hepatology and Infectious Diseases, University Hospital Duesseldorf, Medical Faculty, Heinrich Heine University, Duesseldorf, Germany; [34]Institute of Molecular Medicine, RWTH Aachen University, Aachen, Germany; [35]Institute of Molecular Immunology and Experimental Oncology, Klinikum rechts der Isar, Technical University of Munich, Munich, Germany; [36]Immunology Department, Weizmann Institute of Science, Rehovot, Israel; [37]Cancer-Microbiome Research Division, DKFZ, Heidelberg, Germany; [38]Newcastle NIHR Biomedical Research Center, Newcastle upon Tyne Hospitals NHS Trust, Newcastle upon Tyne, United Kingdom; [39]Emmy Noether Research Group Epigenetic Machineries and Cancer, Division

of Chronic Inflammation and Cancer, German Cancer Research Center (DKFZ), Heidelberg, Germany; [40]School of Biomedical, Nutrition and Sports Sciences, Faculty of Medical Sciences, Newcastle University, Newcastle upon Tyne, UK; [41]Faculty of Biosciences, Heidelberg University, Heidelberg, Germany; [42]North Park University, Chicago, IL, USA; [43]Translational Pancreatic Cancer Research Center, Clinic and Polyclinic for Internal Medicine II, Klinikum rechts der Isar of the Technical University of Munich (TUM), Munich, Germany; [44]M3 Research Institute, Eberhard Karls University Tübingen, Tübingen, Germany

Abbreviations

AID, activation-induced cytidine deaminase; ALT, alanine aminotransferase; BCR, B cell receptor; BMDMs, bone marrow-derived macrophages; CCL2, chemokine (C–C motif) ligand 2; CCl_4, carbon tetrachloride; CCR2, C–C motif chemokine receptor 2; CDA-HFD, choline-deficient amino acid-specific high-fat diet; CD-HFD, choline-deficient high-fat diet; CTLA4, cytotoxic T-lymphocyte associated protein 4; CXCR4/6, C-X-C motif chemokine receptor 4/6; FCER1G, Fc epsilon receptor Ig; FCGR1, Fc-gamma receptor 1; GF, germ-free; HCC, hepatocellular carcinoma; 1H-NMR, proton-nuclear magnetic resonance; ICAM-1, intercellular adhesion molecule 1; IHC, immunohistochemistry; IL-, interleukin-; LFA-1, Lymphocyte function-associated antigen 1; mAb, monoclonal antibody; MHC-I/II, major histocompatibility complex, class I/II; MoMFs, monocyte-derived macrophages; NAFLD, non-alcoholic fatty liver disease; NAS, NAFLD activity score; NASH, non-alcoholic steatohepatitis; ND, normal diet; PD1, programmed cell death protein 1; PDGFRβ, platelet-derived growth factor receptor beta; SAMs, scar-associated macrophages; ScRNA-Seq, single-cell RNA-sequencing; TCR, T-cell receptor; TNF, tumour necrosis factor; t-SNE, t-distributed stochastic neighbour embedding; WD, western diet; WT, wild-type.

Financial support

M.H. was supported by an European Research Council (ERC) Consolidator grant (HepatoMetaboPath), SFBTR179 project ID 272983813, SFB/TR 209 project ID 314905040, SFBTR1335 project ID 360372040, SFB 1479 (Project ID: 441891347), the Wilhelm Sander-Stiftung, the Rainer Hoenig Stiftung, a Horizon 2020 grant (Hep-Car), Research Foundation Flanders (FWO) under grant 30826052 (EOS Convention MODEL-IDI), Deutsche Krebshilfe projects 70113166 and 70113167, German-Israeli Cooperation in Cancer Research (DKFZ-MOST) and the Helmholtz-Gemeinschaft, Zukunftsthema 'Immunology and Inflammation' (ZT-0027). M.H. was also supported together with A.W. by seed funding from HI-TRON. E.K. was supported by the GRK 1482. V.L. was financed by Horizon 2020 grant (Hep-Car), and ERC-CoG (HepatoMetaboPath). D.P. & E.K. were supported by the Helmholtz Future topic Inflammation and Immunology. S.S. was supported by the German-Israeli Helmholtz International Research School: Cancer-TRAX (HIRS-0003), a grant from the Helmholtz Association's Initiative and Networking Fund. Q.M.A. and OG are supported by the LITMUS (Liver Investigation: Testing Marker Utility in Steatohepatitis) project which has received funding from the Innovative Medicines Initiative (IMI2) Program of the European Union under Grant Agreement 777377; this Joint Undertaking receives support from the European Union's Horizon 2020 research and innovation programme and EFPIA. QMA is also supported by the Newcastle NIHR Biomedical Research Centre. N.C.H. is supported by a Wellcome Trust Senior Research Fellowship in Clinical Science (ref. 219542/Z/19/Z). A.W. was funded by the DFG via CRC 1292. Z.A. was funded by the DFG under Germanys Excellence Strategy (EXC 2151) 390873048, SFB1454, SFBTR237 and the GRK 2168. A.D.G was supported by European Respiratory Society/short term fellowship (to A.D.G), Else Kröner Memorial Stipendium (to A.D.G), Werner Otto Stiftung (to A.D.G), Erich und Gertrud Roggenbuck Stiftung (to A.D.G), Hamburger Krebsgesellschaft Stiftung (to A.D.G). E.E. is a scientific cofounder of DayTwo and BiomX, and an advisor to Hello Inside, Igen, and Aposense in topics unrelated to this work.

Conflict of interest

E.K. is employed by Springer Nature; M.J.W. is employed by Roche Diagnostics GmbH;D.P. is employed by Novo Nordisk. The authors declare no conflicts of interest that pertain to this work.

Please refer to the accompanying ICMJE disclosure forms for further details.

Authors' contributions

E.K & V.L. wrote the manuscript, experimental conception & work; S.S. experimental work *in vivo*; O.G. experimental work, histological analysis of human tissue; H.L. experimental work mice & microbiome analysis; M.J.W. experimental work *in vivo*; H.H. experimental work; S.B. experimental work with germ-free mice; J.H. experimental work *in vivo* & analysis of immune cells; D.I. 3D imaging of histological slides; L.Z. metabolomic analysis; A.S–P. analysis of immune cells &; single-cell analysis; R.G. bioinformatic single-cell analysis of mouse data; T.OC. experimental work in mice & provided support with writing the manuscript; A.G. experimental work with Kaede mice & provision of samples; A.S. experimental work & provision of samples; Y.S. bioinformatic single-cell analysis of mouse data; M.G.B. experimental work *in vivo* & flow cytometry analysis; C.R. t-SNE immune cell analysis; D.P. experimental work *in vivo* & flow cytometry analysis; R.O. bioinformatic analysis & experimental work; P.R. experimental work *in vivo* & flow cytometry analysis; M.R. experimental work *in vivo* & flow cytometry analysis; N.R. surgical expertise & provision of human samples; M.E.H. experimental work *in vivo*; M.F. experimental work *in vivo*; N.Y. experimental work *in vivo*; J.J. experimental work *in vivo*; I.S. experimental work *in vivo*; C.F. experimental work *in vivo* & flow cytometry analysis; R.M. experimental work & provision of samples; M.F. experimental work & provision of samples; S.J.W. experimental work flow cytometry analysis; S.C. experimental work & transcriptomic analysis of human samples; J. W–K. transcriptomic analysis of human samples; P.R. transcriptomic analysis of human samples; C.K. histological analysis of mouse samples; T.K. experimental work *in vivo* & flow cytometry analysis; A.L.L. experimental work; S.K. experimental work *in vivo* & flow cytometry analysis; P.S.B. microbiome analysis; K.S. provided support in histological analysis; M.H. provided support with t-SNE immune cell analysis; K.R. bioinformatic analysis; H.Z. provided support with bioinformatic analysis; A.W. experimental work; N.M. experimental work *in vivo*; T.L. conceptual input & provision of samples; M.V. experimental work *in vivo* & provision of samples; H.A. experimental work; R.F. conceptual input, microbiome and IgA analysis; O.P. experimental work *in vivo*; R.R. experimental work *in vivo*; N.H. experimental work *in vivo* & flow cytometry; S.H. experimental work *in vivo*; A.M. provided support with experimental work *in vivo*; P.C. conceptual input & provided support with experimental work *in vivo*; M.C. bioinformatic analysis; A.G. provided human samples; C.T. metabolomic analysis; E.E. conceptual input & bioinformatic analysis; A.E. conceptual input, provision of mice, experimental work *in vivo* & in vitro; Z.A. conceptual input, provision of mice, experimental work *in vivo* & in vitro; D.H. conceptual input, provision of germ-free mice, experimental work *in vivo*; F.T. conceptual input, analysis of myeloid cells, support with experimental work *in vivo*; Q.A. experimental work with human tissues and serum samples & provision of human NASH cohort; M.H. conceptual support & input, wrote the manuscript with E.K. & V.L. and supervised this study.

Data availability statement

The accession number for the bulk RNA-sequencing of sorted intestinal murine CD20+ and CD19+ cells reported in this paper is GSE190691. Data of scRNA-Seq for murine liver and intestine analyses are submitted under GSE131834 and GSE190204, respectively. The accession numbers for human scRNA-Seq sequencing are GSE136103, GSE190487 and GSM5724573. Further information and requests for resources and reagents should be directed to and will be fulfilled by the Lead Contact, Prof. M. Heikenwälder.

Acknowledgements

We thank Danijela Heide, Florian Müller, Enrico Focaccia, Mohammad Ahmed, Sabrina Schumacher, Jenny Hetzer, Corinna Leuchtenberger, Tim Machauer for excellent technical help. Moreover, we are very thankful for the support executed by the Comparative Experimental Pathology laboratory of the Technical University of Munich (TUM). A.W. was funded by the Deutsche Forschungsgemeinschaft DFG via CRC 1292. Z.A. was funded by the DFG under Germanys Excellence Strategy (EXC 2151) 390873048, SFB1454, SFBTR237 and the GRK 2168.

Supplementary data

Supplementary data to this article can be found online at https://doi.org/10.1016/j.jhep.2023.04.037.

References

Author names in bold designate shared co-first authorship

[1] Huang DQ, El-Serag HB, Loomba R. Global epidemiology of NAFLD-related HCC: trends, predictions, risk factors and prevention. Nat Rev Gastroenterol Hepatol 2021;18(4):223–238.

[2] **Anstee QM**, **Reeves HL**, **Kotsiliti E**, Govaere O, Heikenwalder M. From NASH to HCC: current concepts and future challenges. Nat Rev Gastroenterol Hepatol 2019;16(7):411–428.

[3] Pfister D, Núñez NG, Pinyol R, Govaere O, Pinter M, Szydlowska M, et al. NASH limits anti-tumour surveillance in immunotherapy-treated HCC. Nature 2021;592(7854):450–456.
[4] Dudek M, Pfister D, Donakonda S, Filpe P, Schneider A, Laschinger M, et al. Auto-aggressive CXCR6. Nature 2021;592(7854):444–449.
[5] Ringelhan M, Pfister D, O'Connor T, Pikarsky E, Heikenwalder M. The immunology of hepatocellular carcinoma. Nat Immunol 2018;19(3):222–232.
[6] W.H.O. Cancer: key facts. 2020. https://www.who.int/news-room/fact-sheets/detail/cancer.
[7] Llovet JM, Kelley RK, Villanueva A, Singal AG, Pikarsky E, Roayaie S, et al. Hepatocellular carcinoma. Nat Rev Dis Primers 2021;7(1):6.
[8] Schulz M, Tacke F. Identifying high-risk NASH patients: what we know so far. Hepat Med 2020;12:125–138.
[9] Sanyal AJ, Van Natta ML, Clark J, Neuschwander-Tetri BA, Diehl A, Dasarathy S, et al. Prospective study of outcomes in adults with nonalcoholic fatty liver disease. N Engl J Med 2021;385(17):1559–1569.
[10] Piscaglia F, Svegliati-Baroni G, Barchetti A, Pecorelli A, Marinelli S, Tiribelli C, et al. Clinical patterns of hepatocellular carcinoma in nonalcoholic fatty liver disease: a multicenter prospective study. Hepatology 2016;63(3):827–838.
[11] Aby E, Phan J, Truong E, Grotts J, Saab S. Inadequate hepatocellular carcinoma screening in patients with nonalcoholic steatohepatitis cirrhosis. J Clin Gastroenterol 2019;53(2):142–146.
[12] O'Hara J, Finnegan A, Dhillon H, Ruiz-Casas L, Pedra G, Franks B, et al. Cost of non-alcoholic steatohepatitis in Europe and the USA: the GAIN study. JHEP Rep 2020;2(5):100142.
[13] Lazarus JV, Mark HE, Anstee QM, Arab JP, Batterham RL, Castera L, et al. Advancing the global public health agenda for NAFLD: a consensus statement. Nat Rev Gastroenterol Hepatol 2021;19(1):60–78.
[14] De Munck TJI, Xu P, Verwijs HJA, Masclee AAM, Jonkers D, Verbeek J, et al. Intestinal permeability in human nonalcoholic fatty liver disease: a systematic review and meta-analysis. Liver Int 2020;40(12):2906–2916.
[15] Le Roy T, Llopis M, Lepage P, Bruneau A, Rabot S, Bevilacqua C, et al. Intestinal microbiota determines development of non-alcoholic fatty liver disease in mice. Gut 2013;62(12):1787–1794.
[16] **Henao-Mejia J**, **Elinav E**, **Jin C**, Hao L, Mehal WZ, Strowig T, et al. Inflammasome-mediated dysbiosis regulates progression of NAFLD and obesity. Nature 2012;482(7384):179–185.
[17] De Minicis S, Rychlicki C, Agostinelli L, Saccomanno S, Candelaresi C, Trozzi L, et al. Dysbiosis contributes to fibrogenesis in the course of chronic liver injury in mice. Hepatology 2014;59(5):1738–1749.
[18] Yoshimoto S, Loo TM, Atarashi K, Kanda H, Sato S, Oyadomari S, et al. Obesity-induced gut microbial metabolite promotes liver cancer through senescence secretome. Nature 2013;499(7456):97–101.
[19] Kubes P, Mehal WZ. Sterile inflammation in the liver. Gastroenterology 2012;143(5):1158–1172.
[20] **Malehmir M**, **Pfister D**, **Gallage S**, **Szydlowska M**, **Inverso D**, Kotsiliti E, et al. Platelet GPIbα is a mediator and potential interventional target for NASH and subsequent liver cancer. Nat Med 2019;25(4):641–655.
[21] **Wen Y**, **Lambrecht J**, Ju C, Tacke F. Hepatic macrophages in liver homeostasis and diseases-diversity, plasticity and therapeutic opportunities. Cell Mol Immunol 2021;18(1):45–56.
[22] McPherson S, Henderson E, Burt AD, Day CP, Anstee QM. Serum immunoglobulin levels predict fibrosis in patients with non-alcoholic fatty liver disease. J Hepatol 2014;60(5):1055–1062.
[23] Mouzaki M, Bramlage K, Arce-Clachar AC, Xanthakos SA. Serum immunoglobulin A levels do not correlate with liver disease severity in pediatric nonalcoholic fatty liver disease. J Pediatr Gastroenterol Nutr 2018;67(5):631–634.
[24] Shalapour S, Lin XJ, Bastian IN, Brain J, Burt AD, Aksenov AA, et al. Inflammation-induced IgA+ cells dismantle anti-liver cancer immunity. Nature 2017;551(7680):340–345.
[25] Barrow F, Khan S, Fredrickson G, Wang H, Dietsche K, Parthiban P, et al. Microbiota-driven activation of intrahepatic B cells aggravates NASH through innate and adaptive signaling. Hepatology 2021;74(2):704–722.
[26] Karl M, Hasselwander S, Zhou Y, Reifenberg G, Kim YO, Park KS, et al. Dual roles of B lymphocytes in mouse models of diet-induced nonalcoholic fatty liver disease. Hepatology 2022;76(4):1135–1149.
[27] Inamine T, Schnabl B. Immunoglobulin A and liver diseases. J Gastroenterol 2018;53(6):691–700.
[28] Chen J, Trounstine M, Alt FW, Young F, Kurahara C, Loring JF, et al. Immunoglobulin gene rearrangement in B cell deficient mice generated by targeted deletion of the JH locus. Int Immunol 1993;5(6):647–656.
[29] Wolf MJ, Adili A, Piotrowitz K, Abdullah Z, Boege Y, Stemmer K, et al. Metabolic activation of intrahepatic CD8+ T cells and NKT cells causes nonalcoholic steatohepatitis and liver cancer via cross-talk with hepatocytes. Cancer Cell 2014;26(4):549–564.
[30] Komatsu M, Waguri S, Koike M, Sou YS, Ueno T, Hara T, et al. Homeostatic levels of p62 control cytoplasmic inclusion body formation in autophagy-deficient mice. Cell 2007;131(6):1149–1163.
[31] Macpherson AJ, Lamarre A, McCoy K, Harriman GR, Odermatt B, Dougan G, et al. IgA production without mu or delta chain expression in developing B cells. Nat Immunol 2001;2(7):625–631.
[32] **Khodadadi L**, **Cheng Q**, Radbruch A, Hiepe F. The maintenance of memory plasma cells. Front Immunol 2019;10:721.
[33] Szklarczyk D, Gable AL, Lyon D, Junge A, Wyder S, Huerta-Cepas J, et al. STRING v11: protein-protein association networks with increased coverage, supporting functional discovery in genome-wide experimental datasets. Nucleic Acids Res 2019;47(D1):D607–D613.
[34] Gorenshteyn D, Zaslavsky E, Fribourg M, Park CY, Wong AK, Tadych A, et al. Interactive big data resource to elucidate human immune pathways and diseases. Immunity 2015;43(3):605–614.
[35] Tomura M, Yoshida N, Tanaka J, Karasawa S, Miwa Y, Miyawaki A, et al. Monitoring cellular movement *in vivo* with photoconvertible fluorescence protein "Kaede" transgenic mice. Proc Natl Acad Sci U S A 2008;105(31):10871–10876.
[36] Clapper JR, Hendricks MD, Gu G, Wittmer C, Dolman CS, Herich J, et al. Diet-induced mouse model of fatty liver disease and nonalcoholic steatohepatitis reflecting clinical disease progression and methods of assessment. Am J Physiol Gastrointest Liver Physiol 2013;305(7):G483–G495.
[37] Waisman A, Kraus M, Seagal J, Ghosh S, Melamed D, Song J, et al. IgG1 B cell receptor signaling is inhibited by CD22 and promotes the development of B cells whose survival is less dependent on Ig alpha/beta. J Exp Med 2007;204(4):747–758.
[38] Waisman A, Croxford AL, Demircik F. New tools to study the role of B cells in cytomegalovirus infections. Med Microbiol Immunol 2008;197(2):145–149.
[39] Peschl P, Bradl M, Höftberger R, Berger T, Reindl M. Myelin oligodendrocyte glycoprotein: deciphering a target in inflammatory demyelinating diseases. Front Immunol 2017;8:529.
[40] Wei M, Shinkura R, Doi Y, Maruya M, Fagarasan S, Honjo T. Mice carrying a knock-in mutation of Aicda resulting in a defect in somatic hypermutation have impaired gut homeostasis and compromised mucosal defense. Nat Immunol 2011;12(3):264–270.
[41] Harriman G, Bogue M, Rogers P, Finegold M, Pacheco S, Bradley A, et al. Targeted deletion of the IgA constant region in mice leads to IgA deficiency with alterations in expression of other Ig isotypes. J Immunol 1999;162(5):2521–2529.
[42] Muramatsu M, Kinoshita K, Fagarasan S, Yamada S, Shinkai Y, Honjo T. Class switch recombination and hypermutation require activation-induced cytidine deaminase (AID), a potential RNA editing enzyme. Cell 2000;102(5):553–563.
[43] Matsumoto M, Hada N, Sakamaki Y, Uno A, Shiga T, Tanaka C, et al. An improved mouse model that rapidly develops fibrosis in non-alcoholic steatohepatitis. Int J Exp Pathol 2013;94(2):93–103.
[44] Nimmerjahn F, Ravetch JV. Fcgamma receptors as regulators of immune responses. Nat Rev Immunol 2008;8(1):34–47.
[45] Hansen IS, Hoepel W, Zaat SAJ, Baeten DLP, den Dunnen J. Serum IgA immune complexes promote proinflammatory cytokine production by human macrophages, monocytes, and kupffer cells through FcαRI-TLR cross-talk. J Immunol 2017;199(12):4124–4131.
[46] Hansen IS, Baeten DLP, den Dunnen J. The inflammatory function of human IgA. Cell Mol Life Sci 2019;76(6):1041–1055.
[47] Chen L, Li J, Zhang J, Dai C, Liu X, Wang J, et al. S100A4 promotes liver fibrosis via activation of hepatic stellate cells. J Hepatol 2015;62(1):156–164.
[48] **Zheng D**, **Liwinski T**, Elinav E. Interaction between microbiota and immunity in health and disease. Cell Res 2020;30(6):492–506.
[49] Macpherson AJ, Heikenwalder M, Ganal-Vonarburg SC. The liver at the nexus of host-microbial interactions. Cell Host Microbe 2016;20(5):561–571.
[50] Bouter KE, van Raalte DH, Groen AK, Nieuwdorp M. Role of the gut microbiome in the pathogenesis of obesity and obesity-related metabolic dysfunction. Gastroenterology 2017;152(7):1671–1678.
[51] Kübeck R, Bonet-Ripoll C, Hoffmann C, Walker A, Müller VM, Schüppel VL, et al. Dietary fat and gut microbiota interactions determine diet-induced obesity in mice. Mol Metab 2016;5(12):1162–1174.
[52] Fleissner CK, Huebel N, Abd El-Bary MM, Loh G, Klaus S, Blaut M. Absence of intestinal microbiota does not protect mice from diet-induced obesity. Br J Nutr 2010;104(6):919–929.

[53] Kolodziejczyk AA, Zheng D, Shibolet O, Elinav E. The role of the microbiome in NAFLD and NASH. EMBO Mol Med 2019;11(2).
[54] Bäckhed F, Manchester JK, Semenkovich CF, Gordon JI. Mechanisms underlying the resistance to diet-induced obesity in germ-free mice. Proc Natl Acad Sci U S A 2007;104(3):979–984.
[55] Rabot S, Membrez M, Bruneau A, Gérard P, Harach T, Moser M, et al. Germ-free C57BL/6J mice are resistant to high-fat-diet-induced insulin resistance and have altered cholesterol metabolism. FASEB J 2010;24(12):4948–4959.
[56] Moretti CH, Schiffer TA, Li X, Weitzberg E, Carlström M, Lundberg JO. Germ-free mice are not protected against diet-induced obesity and metabolic dysfunction. Acta Physiol (Oxf) 2021;231(3):e13581.
[57] Tacke F. Targeting hepatic macrophages to treat liver diseases. J Hepatol 2017;66(6):1300–1312.
[58] Tacke F, Zimmermann HW. Macrophage heterogeneity in liver injury and fibrosis. J Hepatol 2014;60(5):1090–1096.
[59] Ramachandran P, Dobie R, Wilson-Kanamori JR, Dora EF, Henderson BEP, Luu NT, et al. Resolving the fibrotic niche of human liver cirrhosis at single-cell level. Nature 2019;575(7783):512–518.
[60] **Spencer J**, **Sollid LM**. The human intestinal B-cell response. Mucosal Immunol 2016;9(5):1113–1124.
[61] Rolli V, Gallwitz M, Wossning T, Flemming A, Schamel WW, Zürn C, et al. Amplification of B cell antigen receptor signaling by a Syk/ITAM positive feedback loop. Mol Cel 2002;10(5):1057–1069.
[62] Stepanek O, Draber P, Drobek A, Horejsi V, Brdicka T. Nonredundant roles of Src-family kinases and Syk in the initiation of B-cell antigen receptor signaling. J Immunol 2013;190(4):1807–1818.
[63] Wang WH, Krisenko MO, Higgins RL, Morman RE, Geahlen RL. A mouse model for the study of SYK function through chemical genetics demonstrates SYK-dependent signaling through the B cell receptor, but not TLR4. Immunohorizons 2019;3(7):254–261.
[64] Heizmann B, Reth M, Infantino S. Syk is a dual-specificity kinase that self-regulates the signal output from the B-cell antigen receptor. Proc Natl Acad Sci U S A 2010;107(43):18563–18568.
[65] Gobessi S, Laurenti L, Longo PG, Carsetti L, Berno V, Sica S, et al. Inhibition of constitutive and BCR-induced Syk activation downregulates Mcl-1 and induces apoptosis in chronic lymphocytic leukemia B cells. Leukemia 2009;23(4):686–697.
[66] Friedman SL, Ratziu V, Harrison SA, Abdelmalek MF, Aithal GP, Caballeria J, et al. A randomized, placebo-controlled trial of cenicriviroc for treatment of nonalcoholic steatohepatitis with fibrosis. Hepatology 2018;67(5):1754–1767.
[67] Martínez-Chantar ML, Delgado TC, Beraza N. Revisiting the role of natural killer cells in non-alcoholic fatty liver disease. Front Immunol 2021;12:640869.
[68] Dufour JF, Caussy C, Loomba R. Combination therapy for non-alcoholic steatohepatitis: rationale, opportunities and challenges. Gut 2020;69(10):1877–1884.